EXPERIMENTAL STUDY OF METEOROLOGICAL EFFECTS ON SOLAR SPECTRUM APPLIED TO PREDICT DIFFERENT PHOTOVOLTAIC TECHNOLOGIES

A THESIS SUBMITTED TO THE GRADUATE DIVISION OF THE UNIVERSITY OF HAWAIʻI AT MĀNOA IN PARTIAL FULFILLMENT OF THEREQUIREMENTS FOR THE DEGREE OFMASTER OF SCIENCE IN

ELECTRICAL ENGINEERING

DECEMBER 2010

By

Xi Song

Dissertation Committee:

Eric Miller, Chairperson

Aaron Ohta

David Garmire

Keywords: solar spectrum, photovoltaic technologies, efficiency modeling

ACKNOWLEDGEMENTS

I want to express my sincere appreciation to my advisor Dr. Eric Miller who has inspired me to explore new things both academically and personally. I would also like to thank Dr. Aaron Ohta and Dr. David Garmire for being a part of my dissertation committee and providing me with valuable feedback.

I want to give a special thanks to Dr. Nicolas Gaillard for all the support and for always being open for discussion. I also want to thank the rest of staffs in HNEI Thin Film Lab: Yuancheng Chang, Alexander DeAngelis, Jeremy Kowalczyk, Jess Kaneshiro, Brett Ikei, and Stewart Mallory.

I am grateful to my parents for unconditionally supporting me.

TABLE OF CONTENTS

LIST OF FIGURES

Figure:

LIST OF TABLES

Table:

CHAPTER 1

INTRODUCTION

The natural energy is the most popular and promising resource to use nowadays since the entire world is facing the energy crisis. Renewable energy resources will be an increasingly important part of power generation in the near future. They contribute much necessarily flexibility to the energy resource mix by decreasing the dependence on the traditional fossil-based resources. In addition, they assist in environment protection and reducing the emission of greenhouse gases. As one example of renewable energy utilization, photovoltaic technologies have been used for decades. Due to the increasingly electricity demand, researchers are applying themselves to increase the performance of photovoltaic in terms of efficiency, cost and utilization rate.

This thesis includes two parts of experimental study; one is the measurement and analysis of the solar spectrum and another one is the characterization of spectral response of several kinds of solar cell fabricated with different materials. It is very critical to get a clear idea about the solar resource and the energy conversion potential, especially in unique climates, such as that found in Hawai'i.At the end of the thesis, there is a section about the modeling of a solution for green energy buildings using photovoltaic panels, applying research results from the thesis.

The meaningful achievement for this experimental study is that an empirical estimation of photovoltaic energy conversion can be obtained by generalizing the characteristics of solar spectra and photovoltaic characteristics.

1.1 Background (The Solar Resource)

The background knowledge of the solar resource is necessary to introduce before talking about the solar cell. Nowadays, worldwide database recording solar or other meteorological information is available. However, the impact on the efficiency of photovoltaic conversion depending on the distribution of the solar irradiation and its meteorological effects has not been completely developed. Different materials of solar cells (specified photovoltaic cell) will respond to the different ranges of solar energy. To get the fundamental knowledge about solar irradiance spectrum and solar insolation level will definitely help the solar cell research and development.

1.1.1 Solar Energy related knowledge

Solar radiation emission from the sun into every corner of space appears in the form of electromagnetic wave that carries energy at the speed of light [1]. Depending on the geographical location of the earth and the composition of the atmosphere, the incoming irradiation at any given point appears different shapes in terms of solar spectra.

The solar irradiation energy first interacts with the atmosphere and then reaches to the earth's surface. The atmosphere absorbs approximate two thirds of the incoming irradiation due to water vapor and a lesser degree by CO_2 that exist in the atmospheric composition [2]. Incoming solar irradiance will be shared by cloud and surface reflections. The rest is finally absorbed by the earth's surface. This is this final portion of the solar spectrum that can be used as the resource by photovoltaic panel to generate electricity.

Airmass and Incidence Angle

It is complicated to describe the earth's orbital movement around the sun. This movement affects the climate, solar irradiation and temporal variations. The total amount of the solar irradiation reaching the earth's surface can vary due to these effects. To simplify these variations, the term *Airmass* (abbreviated AM) is used to depict different types of solar irradiance. The solar spectrum is affected by many factors including the solar elevation angle, and the airmass ratio, *m*, can be calculated from different angles of incident light. Although, the solar position is various at any place at any time of day, and the elevation angle also different, using the airmass will uniform all these variable.

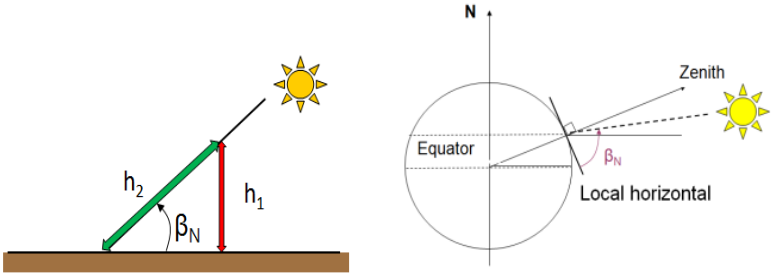

Fig 1.1: The elevation angle of the sun.

The airmass ratio, *m*, is the length of the path h_1 taken by the sun's rays as they pass through the atmosphere divided by the minimum possible path length h_2 [2] (Fig 1.1).

The airmass ratio can be expressed as

Airmass ratio: $$m = \frac{h_2}{h_1} = \frac{1}{\sin \beta_N}$$ Eq 1.1

where β_N is the elevation angle of the sun. AM0 means no atmosphere; it is the extraterrestrial space. AM1 means that the sun is directly overhead. AM1.5 is assumed for an average solar spectrum at the earth's surface [3] and

also considered for standard test of solar device. The solar spectra for various air mass ratios are shown as Fig 1.2.

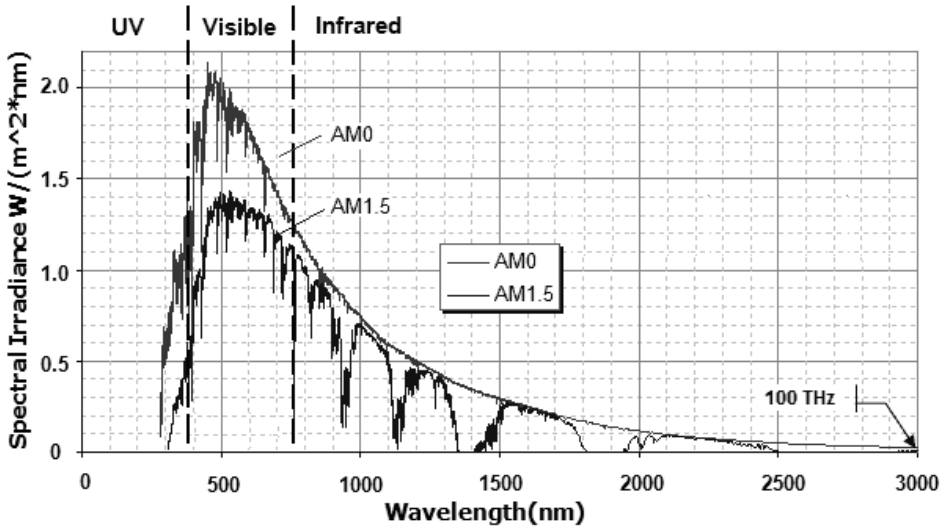

Fig 1.2: Solar spectrum of AM0 and AM1.5.

The portion of incoming solar radiation is also shown in Figure 1.2. With AM1.5, 2% of the incoming solar energy is in the spectrum of Ultra Violet (UV), 54% is in visible light, and 44% is in infrared. However, the largest portion of energy is in the visible range, from 380nm to 780nm [3]. The visible range only accounts for 20% of the whole wavelength range.

Solar Radiation

Solar Radiation from the sun irradiate through space into atmosphere, a certain portion of solar radiation or photons are absorbed by the atmosphere, clouds and particles; another portion is reflected back into space; and other portion is absorbed by the earth's surface. The earth's surface also reflects a certain amount of energy with different wavelength due to the earth's surface temperature [3].

Diffuse radiation -- After the solar radiation enters the atmosphere, it is partially scattered and absorbed by clouds and particles depending on the incidence angle and the wavelength [4]. However, not the entire radiation scattered or absorbed will lost, a part of it will reach the earth's surface as *diffuse radiation*. Because of the uncertainty of cloud cover factor, the diffuse radiation will be variable from day to day. Therefore, it is necessary to measure and record the daily solar irradiance and insolation level for further solar cell analysis usage. It can be seen from the Fig 1.3, the diffuse radiation only contributes a minor portion to the energies from above the mid-visible through to the infrared spectrum, but can contribute up to 40% of the energies from the mid-visible through to the mid-ultraviolet spectrum [5].

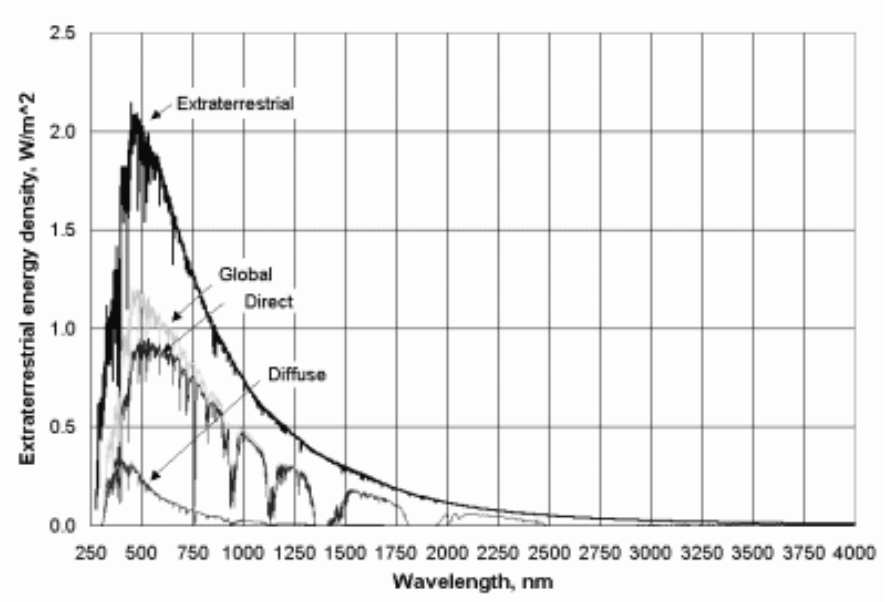

Fig 1.3: Direct, diffuse and total radiation for a standard atmosphere, with relative airmass of 1.5 [5].

Reflected radiation -- It is clear that the quantity of solar radiation reaching any particular place of the earth is determined by the position of the point, time of year, atmosphere diffusion and absorption, cloud cover and shape of the surface. The terrain like mountainous will also reflect the radiation as called *reflected radiation*. For the record, some of the structural issue will also reflect the solar radiation as commonly occurring on the roof of the building which is the location for PV panel installation.

Direct radiation or called *Beam radiation* is that the solar radiation travels straightly into atmosphere and reach to the earth's surface without any disturbances. Direct radiation can be further reflected and diffuse by the surfaces.

Global radiation or *total radiation* is the sum of diffuse radiation, reflected radiation and direct radiation. The most common measurements of solar radiation by spectroradiometer are global radiation, and it is always expressed as the irradiance as the function of wavelength. As we can seen from Figure 3 above, the wavelength range can reach to 3000nm, but from the experimental measurement, the equipment can only measure the wavelength until 1100nm which is the major range of solar cell absorption.

1.1.2 Solar Constant, Solar Irradiance Spectrum and Solar Insolation

The solar constant is the extraterrestrial irradiance of the solar beam at mean solar distance. The accepted value is 1367 W/m^2 [5]. This value can be considered as the most value reaching to the earth and can be achieved by the photovoltaic.

The *solar irradiance spectrum* and solar *insolation level* impact the performance of solar panels which usually have a narrow band over which they operate at peak performance. Atmospheric elements like cloud cover,

pollution, aerosols, and volcanic gasses can alter this incident solar spectrum and reduce the solar insolation. It is therefore important to study spectral changes as a function of weather conditions throughout the day. Places like Hawai`i have unique environmental characteristics with locations where rain falls often throughout the year.

The solar incident is subjected to many absorption, diffusion and reflection; therefore, it is necessary to address the total value of the energy brought from the solar radiation.

The term "spectral irradiance" describes the amount of solar power available in a certain area at a certain wavelength ($W/m^2/nm$) and "solar insolation" describes the integrated radiation over all wavelengths of light and describes the power density (W/m^2).

1.1.3 Solar position of any time of the day

To make the experimental measurement uniform, the airmass ratio was used to record the spectra results. The calculations have been done as in Table 1 below for the one day in December. It is seen from the table, the most approached time with AM1.5 occurred at 14:00.

Table 1.1: Air mass ratio measured in Dec. at Hawai`i

Time	Shadow length $\times h_1$	Elevation angle β_N °C	Air mass ratio AM
8:30	3.05	18.16	3.2
9:30	1.80	29.02	2.1
10:30	1.28	38.00	1.6
11:30	1.04	44.01	1.4
12:00	0.97	45.85	1.4
13:00	0.99	45.15	1.4
14:00	1.19	39.99	1.5
15:00	1.63	31.54	1.9
16:00	2.61	21.00	2.8

1.2 Basic Semiconductor Physics

1.2.1 The Band-gap Energy

The solar cell (photovoltaic) uses semiconductor materials to convert solar energy into electricity. As in the solid-state physics, there is an important scale factor of semiconductors' properties, *band-gap.* Band-gap is an energy range in a solid where no electron states can exist. The Fig 1.4 below shows the structure of semiconductor material with the comparison of insulator and conductor, the top energy band is called the conduction band where is the minimal-energy state in, and it is electrons within this region that contribute to current flow. The valence band is the highest range of electron energies where electrons are normally present at absolute zero temperature. The band-gap generally refers to the energy difference between the top of the valence band and the bottom of the conduction band in semiconductor [6]. The gaps

between allowable energy bands are called forbidden bands. The energy that an electron must require to jump across the forbidden band to the conduction band is called the band-gap energy, designed *Eg*. The unit of the band-gap energy is electron volt (eV) (1 eV=1.6*10^{-19} J).

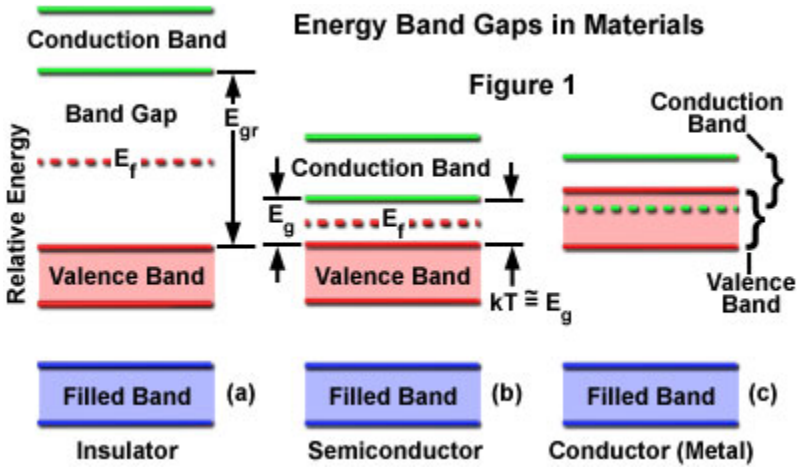

Fig 1.4: The energy band in materials [6].

For the record, the different semiconductor materials have different band-gap *Eg*. The band-gap for silicon is 1.12 eV [6], which means an electron needs 1.12 eV energy to let itself free from the electrostatic force and jumps to the conduction band. The photon energy has an inverse ratio with the wavelength. The calculation is showed below:

$$E_g = h\nu = \frac{hc}{\lambda} \qquad \text{Eq 1.2}$$

Where ν is the frequency, c is the speed of light $\left(3 * 10^8 \frac{m}{s}\right)$, λ is the wavelength, h is Planck's constant.

Fig 1.5 below shows the curve of the irradiance as the function of photon energy. This curve will be used to compare the different photovoltaic materials with different band-gap energy and calculate their electrical parameter.

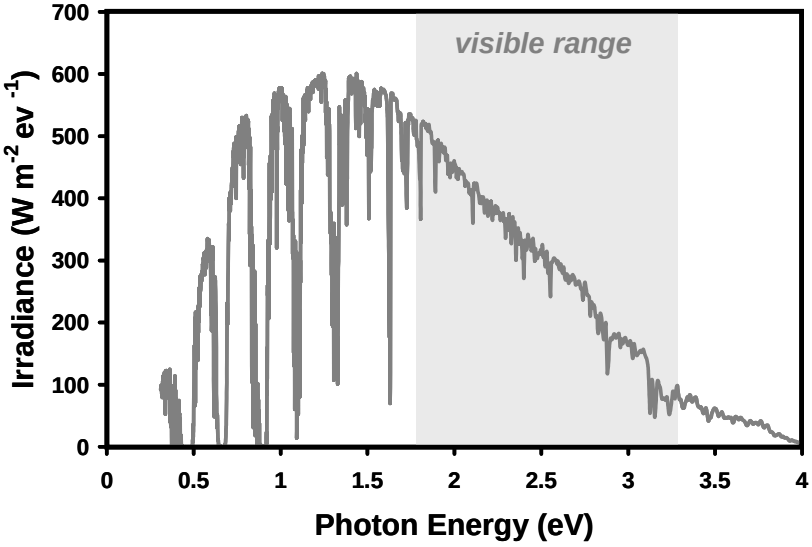

Fig 1.5: The spectrum of irradiance as a function of photon energy.

Take the silicon photovoltaic cell for example: the band-gap for silicon is 1.12 eV, the material can only respond $h\nu > E_g$. Thus, all energy above the Si cut-off wavelength (1100nm) is not absorbed and just heats the photovoltaic cells.

1.2.2 The band-gap structure and light absorption coefficient

Recall that there are two energy states in semiconductor relevant to photovoltaic applications, conduction band and valence band, are each characterized by a certain wave vector *k* defining the *crystal momentum*. *p=hk* If the k-vectors are the same, it is called a "*direct band-gap*". If there are not the same, it is an "*indirect band-gap*" [7].

In direct band-gap semiconductors, such as GaAs, Cu(InGa)Se_2 and CdTe, the electrons can shift from the conduction band to the valence band

without a change in crystal momentum. The arrow in the Fig1.6 is a transition in which a photon excites an electron from the valence band to the conduction band. Assume that every initial electron state with energy E_1 and crystal momentum p_1 in the valence band is associated with a final state in the conduction band at energy E_2 and crystal momentum p_2. Since the electron momentum is conserved, the final state of the crystal momentum is the same as its initial state, $p_1 = p_2 = p$. [6]

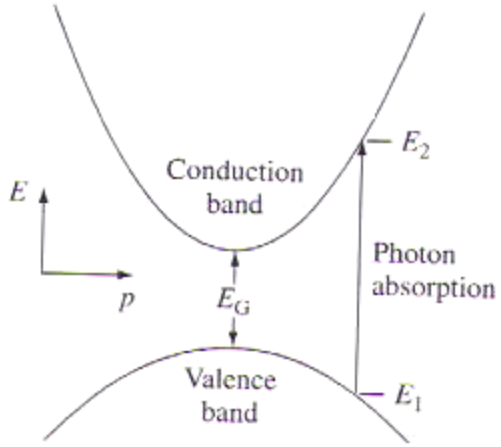

Fig1.6: Photon absorption in a direct band-gap semiconductor for an incident photon with energy $h\nu = E_2 - E_1 > E_G$ [8]

In indirect band-gap semiconductor, such as Si and Ge, where the valence band maximum occurs at a different crystal momentum than the conduction band minimum. It means that an electron cannot shift from the lowest-energy state in the conduction band to the highest-energy state in the valence band without a change in momentum. Notice that it is necessary to involve an additional particle into the absorption process rather than photon, and this additional particle is *phonon* [8]. Phonon is the particle represents lattice vibrations in the semiconductor, and it has low energy but with high momentum. The Fig1.7 below shows that the vertical arrow represents the

photon absorption while the horizontal arrow represents both phonon emission and phonon absorption.

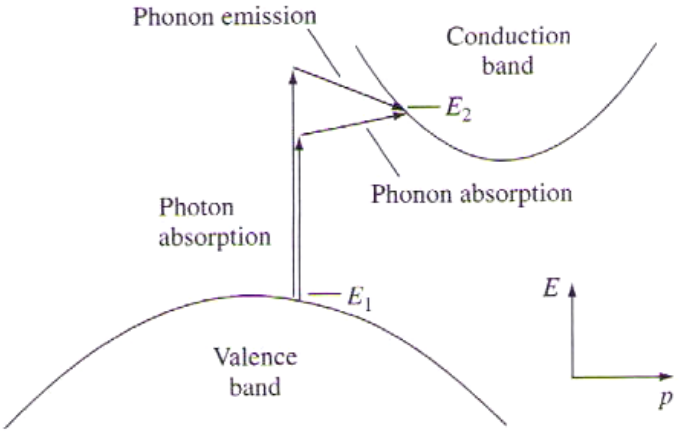

Fig1.7: Photon absorption in an indirect band-gap semiconductor for a photon with energy $hv > E_2 - E_1$. Energy and momentum in each case are conserved by the absorption and emission of a photon [8].

The light absorption coefficient α, is a property of a material that defines the total amount of light absorbed by it. Here in semiconductor, $\alpha(hv)$ is commonly used. The absorption coefficient determines the depth of the light penetration into the semiconductor with a particular wavelength before being absorbed. Compare with the both direct and indirect band-gap, the absorption coefficient for indirect band-gap is relatively small. In other words, in a material with a low absorption coefficient, light is poorly absorbed, and if the material is thin enough, it will appear transparent to that wavelength. The absorption coefficient depends on the materials and also on the wavelength of the light. The absorption coefficient of several semiconductor materials is shown below in Fig 1.8.

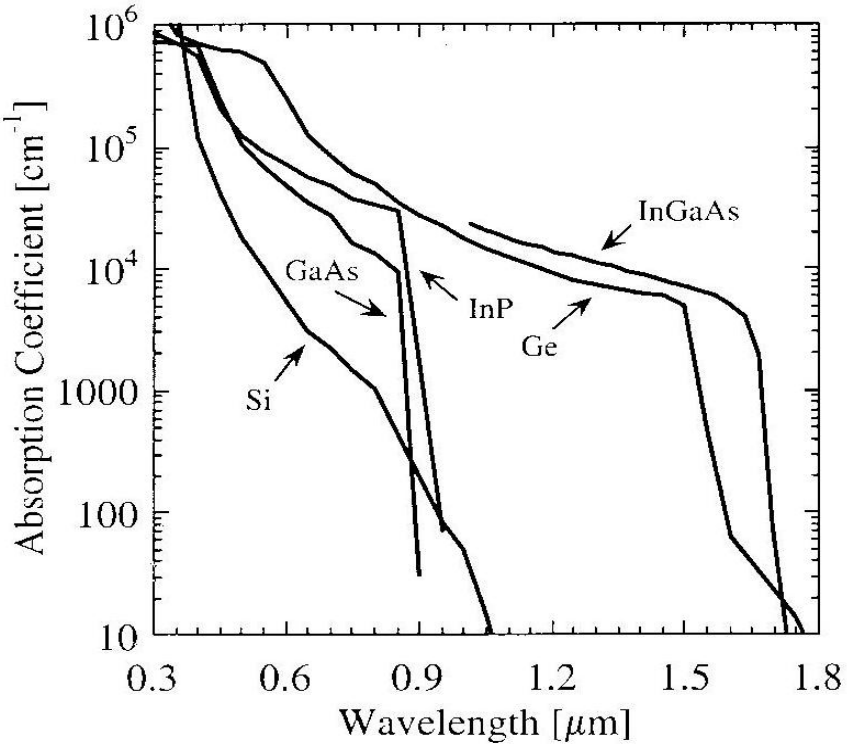

Fig 1.8: The absorption coefficient of several semiconductor materials [9].

The expressions of absorption coefficient for both direct and indirect band-gap are shown below.

Electrons in the valence band of a semiconductor can absorb photons whose energy are higher than the band-gap energy, *Eg*, and jump to the conduction band. The absorption coefficient, *α(E)*, for an energy E higher than the bandgap energy is given by [10]

For a direct semiconductor: $$\alpha(E) = \alpha_0 \sqrt{\frac{E - E_g}{E_g}}$$ Eq 1.4

For an indirect semiconductor: $$\alpha(E) = \alpha_0 \left(\frac{E - E_g}{E_g}\right)^2$$ Eq 1.5

Here, E is the photon energy corresponding to the incident light spectrum by $E = hc / \lambda$.

These two equations allow us to determine the parameter α_0 with is the basis of a simple analytic expression for the absorption coefficient as a function of energy, $\alpha(E)$. Finally we determine α_0 for various direct-gap and indirect-gap semiconductor materials.

1.2.3 Band-gap Impact on Photovoltaic Efficiency

It is very obvious that the band-gap of the semiconductor materials is a crucial constraint for the performance of photovoltaic cell. Even it has a small band-gap, silicon cannot convert the total solar energy to electricity above the cut-off wavelength due to its crystal structure. When a photon with more than 1.12eV is absorbed by a photovoltaic cell, a single electron may jump to the conduction band, which creates hole-electron pairs. But a small band-gap means that more photons have surplus energy above the threshold needed to create hole-electron pairs, which wastes their potential. In other words, a small band-gap gives more current with less voltage. Band-gap in the 1.2eV to 1.8eV range is usually considered as optimum for single junction solar cell [8]. To estimate a more accuracy electricity conversion of photovoltaic cell, the other optical properties will be introduced in next chapter.

The p-n Junction Diode

It is already known that a photovoltaic cell respond to the photons with energies above their band-gap energy and hole-electron pairs will be created. To avoid these charge carriers to recombine, a constant electric field must be created to pull the charges away from each other. For photovoltaic cell

semiconductors, the most common device structures are the p-n junctions. A typical p-n junction photovoltaic cell structures are shown below in Fig1.9

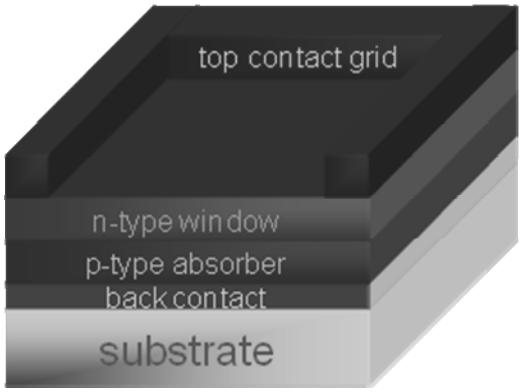

Fig 1.9 A typical p-n junction photovoltaic cell structure [11].

To simplify the photovoltaic cell to a conventional p-n junction diode, the characteristic is shown in Fig1.10

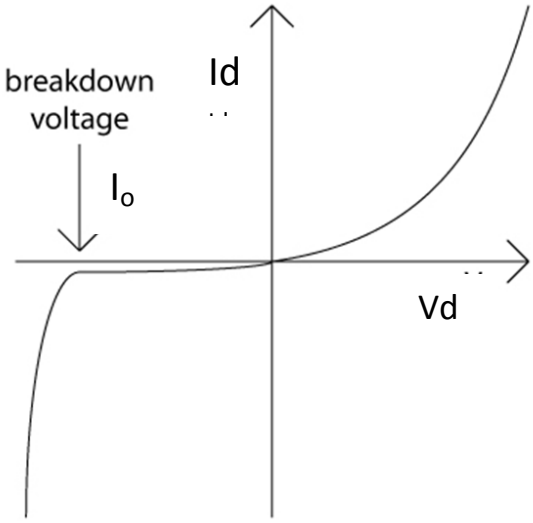

Fig 1.10: The characteristic of p-n junction diode.

The Fig1.10 shows the voltage-current characteristic curve for the p-n junction diode, described by the following Shockley diode equation [12]:

$$I_d = I_0\left(e^{qV_d/kT} - 1\right) \quad \text{Eq 1.6}$$

Where I_d is the diode current, V_d is the voltage across the diode, I_0 is the reverse saturation current, q is the electron charge (1.602*10-19C), k is Boltzmann's constant (1.381*10-23 J/K), and T is the device temperature (K). To simplify the equation as the standard temperature (at 25 ° C).

$$I_d = I_0\left(e^{38.9V_d} - 1\right) \quad \text{Eq 1.7}$$

This is a very important equation in the Equivalent Electrical Circuit. More details will be discussed in Chapter 5.

1.2.4 The Basic structure of solar cell

Generally, there are two types of solar cell structure as shown in Fig 1.11, a) is a superstrate device and b) is a substrate device. Superstrate devices are made on a transparent substrate such as glass, so that the light enters the absorber through the first deposited layer (emitter or buffer). Substrate device are made on both the opaque substrates such as metal foils or metalized glass and transparent glass, and the light enters the absorber through the top deposited layer.

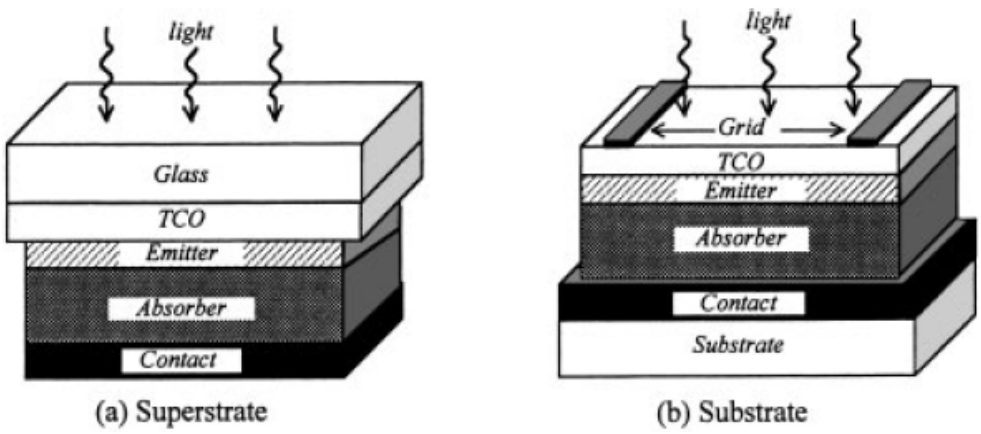

Fig 1.11: Typical superstrate (a) and substrate (b) thin film solar cell configurations [13].

For the convenience of testing, the substrate structures are commonly used in the libratory research. The core part of the solar cell is the absorber and emitter; these are the two components to compose the p-n junction. Different pairs of materials and different integrations are used to form the p-n junctions. Their selection depends first and foremost on process (temperature limitations, deposition methods) and chemical (interface alloying, impurity diffusion) compatibilities. For example, a typical CIGS based solar cell has a substrate device structure of glass/Mo/Cu(InGa)Se2/CdS/ZnO/grid [13], and a CdTe based solar cell have a superstrate device structure of glass/SnO2/Cds/CdTe/metal. For the record, in the fabrication process the thickness of different layer and the different doping rate can lead a significant variation on the performance of the solar cell. But the critical parameter is the absorber layer, where the photo-generation and most of the recombination occurs. So that, the devices are normally be referred to by their absorber layer. The conclusions presented in this thesis are all based on the absorber materials. More characteristics will be discussed in next few chapters.

Chapter 2

Introduction of Several Photovoltaic Materials and Their Main Optical Characteristics

In this chapter, the main semiconductor optical characteristics will be discussed through three different types of thin-film solar cell materials, amorphous silicon (a-Si), CdTe and Cu(In, Ga)Se2 (CIGS).

Recall that, in the structure of the solar cell, the absorber plays the main role, governing the performance of the solar cell. Due to the different properties of the absorber materials, these solar cells will appear different characters. The most common industrial photovoltaic material is silicon or abbreviated to Si. There are many types of silicon solar cell in the market, which dominated by crystalline silicon (s-Si) and polycrystalline silicon (p-Si). Under development, amorphous silicon (a-Si) is a potential lower cost implementation of Si. The number of companies producing the silicon based PV module has grown rapidly since 2005 [14]. The Fig2.1 (a) shows the schematic of single-junction a-Si structure. The majority of silicon based solar cell developers offered the glass module designs and achieved the stabilized efficiencies from 6% for single-junction a-Si and 9% for multi-junction. As of 2010, solar cell manufacture companies have struggled to achieve the profitability due to the cost of materials, low module efficiency, and limited market. Due to this problem, some other potential materials have been considered as commercial product as well.

Cadmium telluride (CdTe) is considered to be one of the promising thin-film materials for the fabrication of solar cell. Commercially, CdTe PV

modules have seen the greatest success among thin-film PV technologies to date. In 2009, commercial CdTe module sales surpassed 1,000MW [14]. A standard superstrate structure as shown in Fig2.1 (b).

During 2003 and 2004, copper indium gallium diselenide (CIGS) has attracted significant interest of both the solar cell manufactories and researchers. The active layers of the CIGS substrate device structure is shown in Fig2.1 (c). Since then, the CIGS-based development has grown tremendously. As in 2010, the efficiencies is greater than 10% (over 13% for 1" by 1" module and 20% at lab-scale) [14].

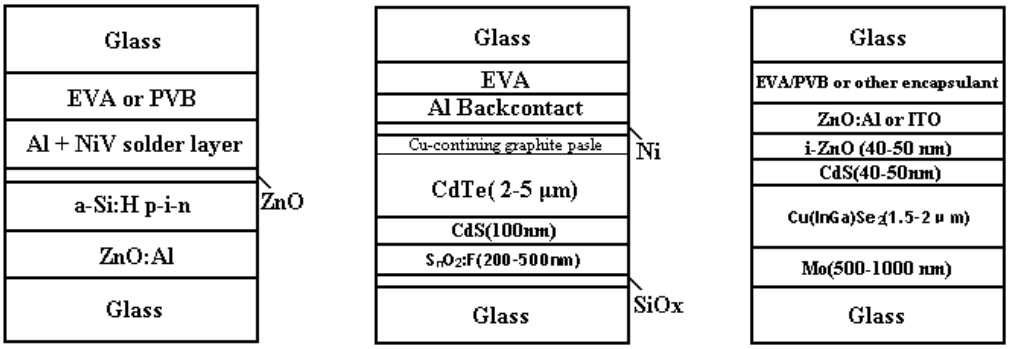

a b c

Fig2.1:a) Schematics of example commercial thin-film silicon PV module device structures. A single-junction a-Si PV module. b) Schematics of example commercial CdTe module device structures. C) Schematics of example commercial CIGS module device structures.

2.1 Transmittance, Reflectance and Tauc Plot

The most basic optical property of solar cell in the context of design and operation is its light absorption properties. These are characterized by a

wavelength-dependent absorption coefficient, as mentioned in chapter 1. To determine the absorption coefficient, the optical transmittance measurement through the certain layer can be applied. The transmittance and reflectance property is another way to describe the light absorbing ability of solar material. Compare with the light absorbance, the transmittance and reflectance will appear a more intuitive look in terms of as combine with the solar spectra. In solar cell performance characterization, we seldom use the transmittance and reflectance properties to analyze the device since the deposited devices have more than one layers and it will disarrange the curve. However, it can be used to identify the value of band-gap of the certain materials.

Tauc plot is a method to calculate the band-gap of semiconductor materials using transmittance or reflectance characteristics [15]. This is a very straightforward calculational method to estimate the optical property of an unknown solar cell material or the different doping rate of the alloys. According to the different band-gap structures in terms of direct band-gap and indirect band-gap, the calculation formulas are not the same. The relationship between absorption coefficient α and band-gap energy Eg [16]:

For direct transitions: $\alpha\ (hv)=A(hv-Eg)^{1/2}$ Eq 2.1

For indirect transitions: $\alpha\ (hv)=A(hv-Eg)^{2}$ Eq 2.2

Where A is a constant which is different for different transitions, Eg is the direct or indirect band-gap of the materials, hv is the incident photon energy.

Amorphous silicon does not have a clearly defined band structure and behaves much like a direct semiconductor since the conservation of momentum is not required [16]. Its band-gaps depend on how the substance is alloyed and can range from 1.4eV to 1.8eV. Fig2.2 shows a typical indirect Tauc Plot. Accordingly for the smaller values of absorption coefficient (αhv)1/2 is plotted against the photon energy. The straight-line portions are

extrapolated to zero and the values obtained are taken as the absorption edge for indirect transition [17].

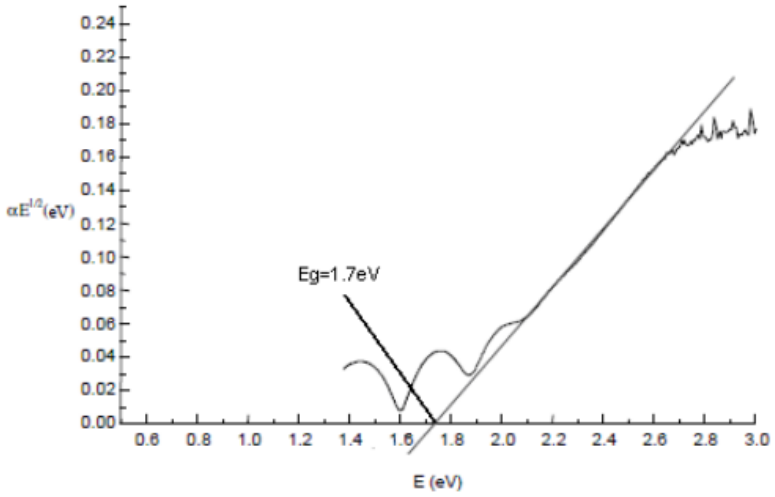

Fig2.2: Tauc plot of a-Si [16].

Another absorber material, CdTe, has a more complicated band structure. It has a high absorption coefficient in the visible range of the solar spectrum and its band-gap (=1.45eV) is close to the optimum value for efficient solar energy conversion [17]. Due to the different thickness deposited at room temperature (Fig2.3 shows the transmittance curve of CdTe with different thickness), it has been observed that the direct band-gap decreases with increasing thickness and it is also found to have direct and indirect band-gap in the same sample. Fig2.4 shows the absorption spectra of CdTe film [18]. It is obviously seen that absorption spectra decreases very sharply at two places with increases in wavelength. This indicates the existence of two band-gaps. Therefore, the direct transition occurs with the higher values of absorption coefficient than indirect transition. Thus, the minimum value αi is substracted from the measured or calculated α. The values of $((\alpha-\alpha_i)hv)^2$ are plotted

against photon energy. Using the same method, the direct band-gap can be observed from Fig2.5.

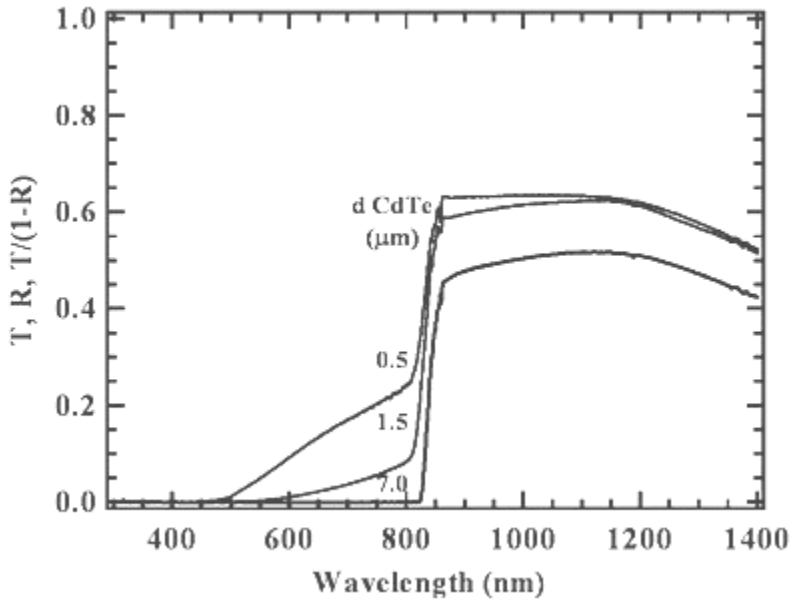

Fig2.3: The transmittance curve of CdTe with different thickness [19]

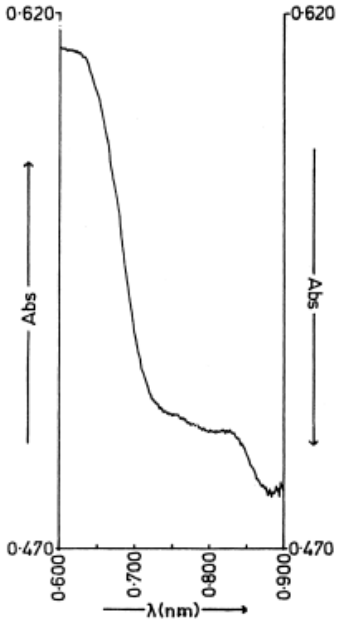

Fig 2.4: Absorption spectra of CdTe film [18]

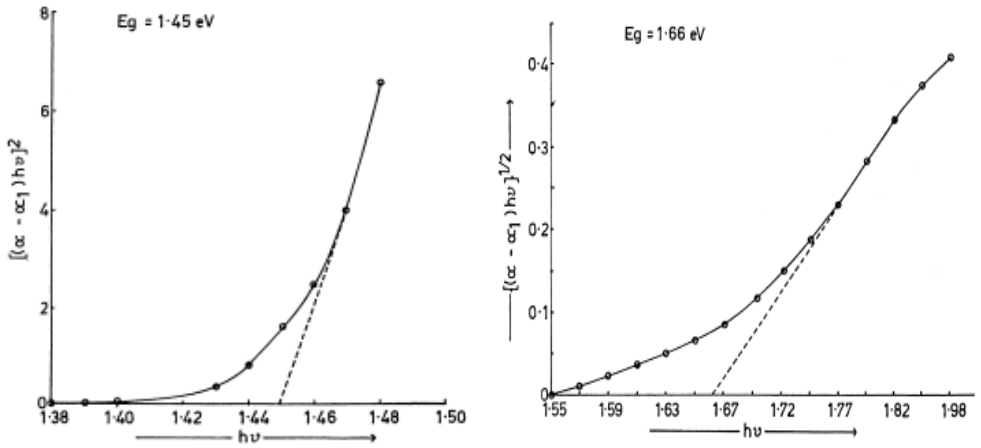

a b

Fig2.5: a) Direct energy band-gap plot. b) Indirect energy band-gap plot [18].

CIGS solar cell has a direct band-gap at 1.15eV [20]. More optical properties about CIGS will be expressed with Quantum Efficiency.

2.2 Quantum Efficiency

Quantum Efficiency (QE) is a quantity defined for a photosensitive device as the percentage of photons hitting the photoreactive surface that will produce electron-hole pair. For solar cell, the quantum efficiency is a very important parameter as it provide the information that how many percentage of light will convert to electron when the given cell illuminated by a particular range of solar spectrum. If the quantum efficiency with a certain solar irradiance is integrated over the whole solar spectrum (for example AM1.5G), the device current density can be estimated.

Quantum Efficiency measurements are commonly used to determine the device losses, especially the optical losses. In general, the primary impact

factor making the differences in shape and cut-off wavelengths is related to the absorber band-gap. Fig2.6 shows the QE of several types solar cells.

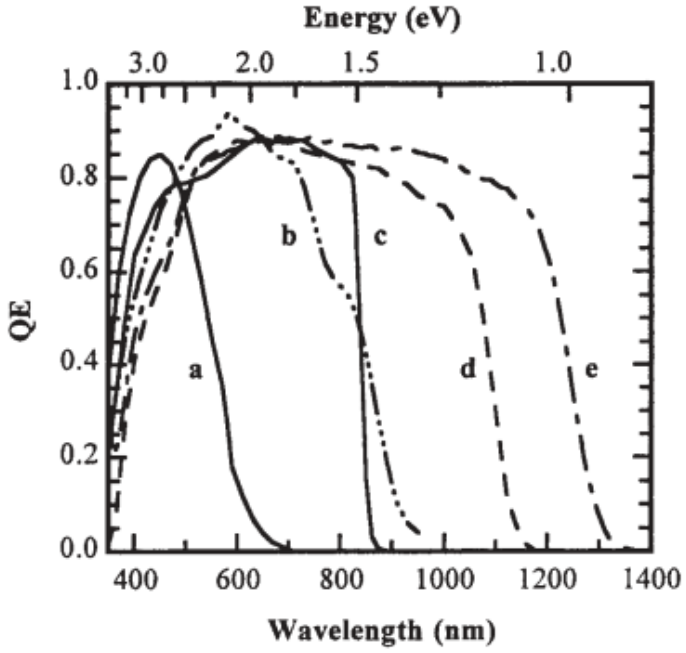

Fig2.6: QE curve of several types of solar cell: a. a-Si, b. a-SiGe, c. CdTe, d. CIGS, e. $CuInSe_2$ [13].

Due to the shading from the collection grid, the QE curves cannot reach to 100% level, and this is the only wavelength-independent optical loss (shading effect). Since the solar cell has a multilayer structure, the shape and magnitude of QE curve at short wavelengths is related to the device structure and window layers. In practice, the magnitude of each of these losses will depend on details of the device design and optical properties of the specific layer. As in CIGS solar cell, the reason making the curve more like triangle rather than a regular trapezium or a quadrangle is due to the combination effect of different layers. The losses in details:

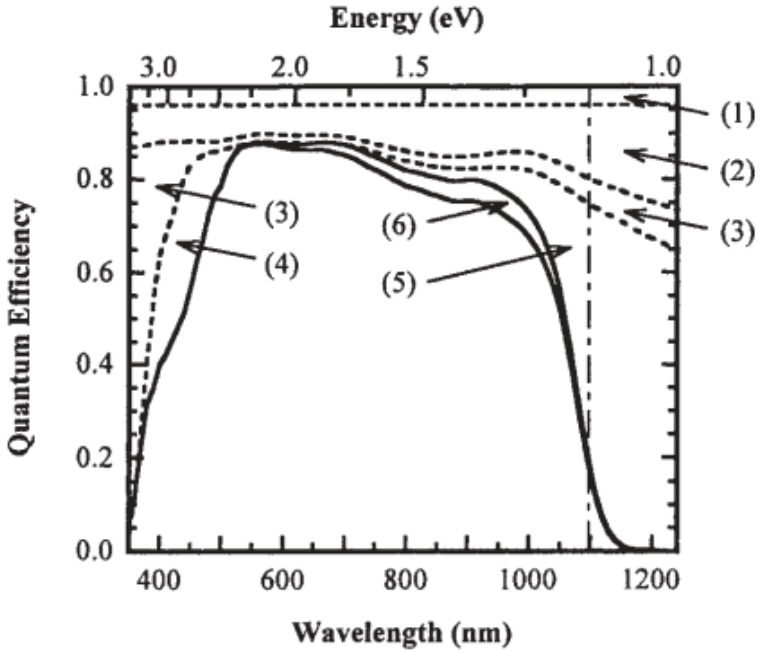

Fig2.7: Quantum efficiency with optical losses for a CIGS solar cell [13].

1. Shading effects for some substrate devices.

2. The reflection of front surface from air/ZnO/CdS/CIGSe interfaces (a substrate type). A typical reflection will reduce the entire magnitude of the QE curve through the wavelength. This can be minimized with an anti-reflection layer.

3. Absorption in the TCO layer and emitter layer (CdS). Typically there is 1-5% absorption by TCO through the visible wavelengths (λ < 400nm) approaching the TCO band-gap.

4. According to the CdS band-gap 2.42eV, the absorption loss in QE for λ < 500nm is inversely proportional to the layer thickness. This is the reason making the QE curve steeper at short wavelengths.

5. Incomplete absorption in the absorber layer. This affects the steepness of the long-wavelength part of the QE curve.

6. Incomplete collection of photogenerated carriers in the absorber. This is the only electrical loss factor with QE.

Table2.1 summarizes these effect factors and this will be an important reference aspect in the following chapters. The real-time solar spectra and laboratory QE measurement will be used to estimate the current density which is a decisive electrical property of solar cell.

Table2.1: Photocurrent loss due to the optical and collection losses for the CIGS. J=42.8mA/cm2 is the total photocurrent available for the AM1.5 spectrum for E>1.12eV [13].

Region in Figure 3	Optical loss mechanism	ΔJ (mA/cm^2)
1	Shading from grid with 4% area coverage	1·7
2	Reflection from Cu(InGa)Se_2/CdS/ZnO	3·8
3	Absorption in ZnO	1·9
4	Absorption in CdS	1·1
5	Incomplete generation in Cu(InGa)Se_2	1·9
6	Incomplete collection in Cu(InGa)Se_2	1·0

Chapter 3

Experimental Measurement of Solar Spectrum and Solar Insolation in Hawai'i

3.1 Experiment Arrangement

3.1.1 Introduction of the sensors

The measurement of the solar spectrum and solar insolation should consider several aspects such as weather conditions, ambient temperature, and the various atmospheric conditions [21]. The spectroradiometer we have been used was made by International Light Technologies, Model Number ILT-900 (http://www.intl-lighttech.com/). The measurement spectral range is from 250nm to 1100nm. It comes with a main silicon photosensitive sensor and a photo-detector data acquisition box which are connected by an optical fiber. The entire system need to communicate with a computer via usb port to accomplish the data acquisition function. A Data achievement and record software is also provided by the company. From this computer interface, the solar spectrum can be measured and downloaded into an Excel spreadsheet for further application.

Due to a limitation of the spectroradiometer, the solar spectrum cannot be recorded as continuous data, but several time points to take the measurements can be chosen according to the weather forecast. The spectroradiometer used in the experiment is shown in Fig 3.1.

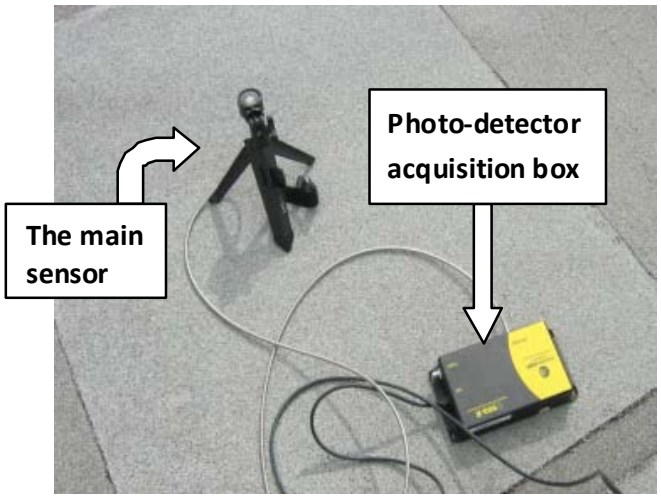

Fig 3.1: The whole set of the spectroradiometer

To calibrate the spectroradiometer, the reference AM1.5 spectrum from the American Society for Testing and Materials (ASTM) was used [5]. The AM1.5 spectrum, occurring at solar noon, corresponds to an insolation of approximately 1000W/m^2. But at different times during the day and due to weather conditions, the real insolation is always less than this value.

Typical solar spectra taken by the spectroradiometer are shown in Fig 3.2 and Fig 3.3.

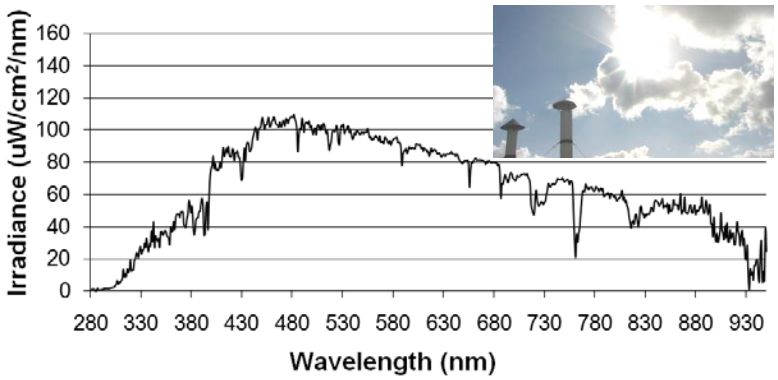

Figure 3.2: The spectra with corresponding sky pictures on a partly cloudy day.

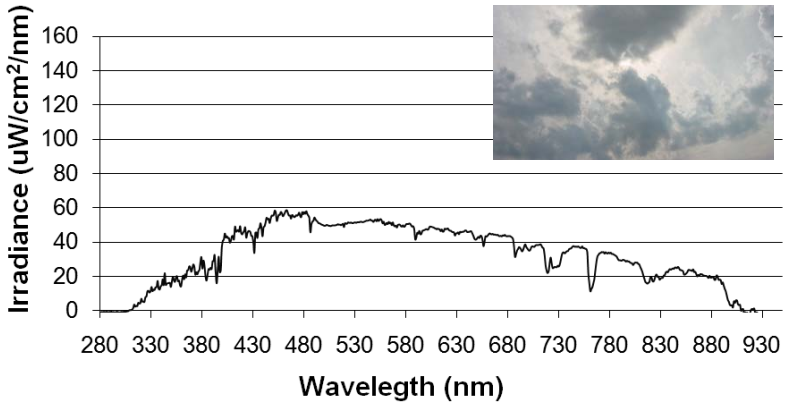

Figure 3.3: The spectra with the corresponding sky pictures on a cloudy day.

The other sensor have been used in the measurement is the pyranometer [22]. A typical pyranometer is made with a silicon photodiode sensor. Depending on different accuracy and durable ability, the pyranometer can be classified into three different levels (Secondary, first class and second class) in terms of the accuracy and measuring scope. The model we used is second class. Fig3.4 shows the comparison of spectroradiometer and pyranometer used in this study.

Fig3.4: The pyranometer and the comparison with the radiometer.

Unlike the spectroradiometer, the pyranometer is more durable and convenience to use. It is designed for long-term measurement and also weather-proof. However, the pyranometer only measures an integrated spectrum value as insolation, as opposed to the full spectral resolution of the spectroradiometer.

Two typical solar insolation level plots in a sunny day and a rainy cloudy day are shown in Fig3.5. The lighter bars represent the rainy and cloudy day while the darker bars represent the sunny day.

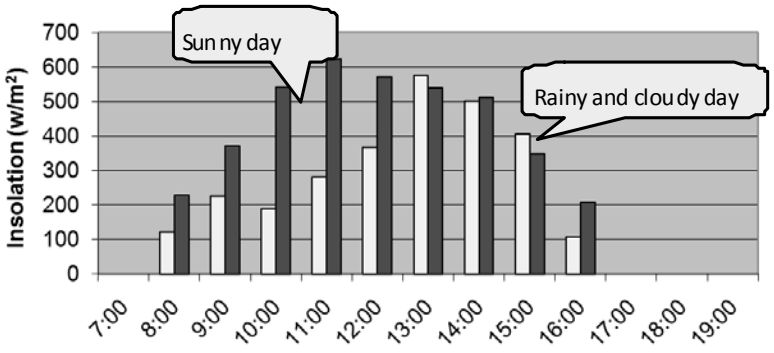

Fig 3.5: Two days of different weather conditions

For temperature measurements, two types of sensors will be introduced here. Handheld thermocouple is a convenience device to measure the ambient temperature. Another type of temperature sensor is used to measure the surface temperature, called “Surface Thermocouple with Self-Adhesive”. This kind of sensor is ideally to measure the temperature of the photovoltaic panels. For the record, this temperature is a crucial parameter in the simulation of photovoltaic device in chapter 5. More details will be discussed later.

3.1.2 Data Acquisition System

Beside of these two types of solar measurement sensors, a data acquisition system must be used in the measurement and it also play an important role in the entire experimental measuring processing.

The data acquisition system used is based on the "compact real-time controller" platform or cRIO from National Instruments company (http://www.ni.com/), shown in the left circle in Fig 3.6. The NI cRIO embedded real-time controller is part of the high-performance CompactRIO programmable automation controller (PAC) platform. The software Labview was used to program the cRIO system for data collection.

To achieve the data measured from the sensors, some of the add-on modules are required. Since the pyranometer is an analog signal output sensor, it needs an analog input module to communicate with the cRIO, shown in the right circle in Fig3.6. Also there is a Thermocouple (TC) module to gather data from thermocouple.

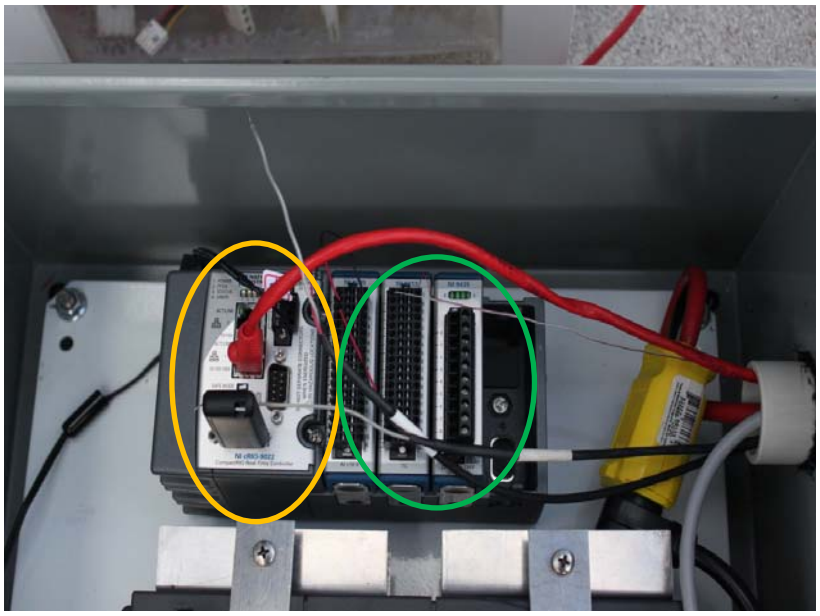

Fig3.6: The details about the cRIO system.

3.1.3 Experimental Setup

The whole system is located on the roof of UH engineering building. In the trial period, the system has to be supplied by the external power and temporarily be mounted on the ground. All the equipments are weather-proof and durable. The Fig3.7 shows the main part of the system expect the pyranometers.

Fig 3.7: The entire Data Acquisition System

The whole system includes a server computer which is showing as this transparent aquarium in the picture. This computer is connecting to the internet so that we can remote control the entire system and download the data to our local computer without going up to the roof.

There are two components in this metal box, one is the cRIO and functional modules, the other one is the power backup which is providing the power supply for the entire system.

3.2 Solar Data Analysis

3.2.1 Key features of solar radiation in different sky conditions

According to the different weather conditions, three basic weather/sky conditions can be identified: cloudy, partly cloudy and sunny. The primary cause of the variability in solar radiation is the cloud coverage, and this effect can be variable due to the different geographic locations. In desert climates [23], there may not be any cloud coverage for long period. In high latitude climates, overcast or cloudy days may persist in winter with only rare breaks of sunshine. Such statistics can be achieved from many resources and also can be forecast or estimate easily.

However, sometimes the cloud coverage can change irregularly in the tropical climates such as in Hawai'i. Recall that the global radiation may be split into two main components, direct radiation and diffuse radiation. The cloudless sky global radiation may be counted as direct radiation except dust (form volcanic ash for example), pollution and water vapor in the atmosphere. There is no direct beam and the radiation is not steady during overcast periods. Changes in the cloud coverage can make the irradiation variable during the day but it tends to be far less than with partly cloudy sky. The cloud can interrupt the direct beam, so the direct irradiance is quite variable during the partly cloudy period. Dramatic changes in direct radiation can occur within a few seconds [24]. The sky can be relatively bright with a lot of scattered cloud, and the associated diffuse irradiation can be quite large during such period. However, the short-term variations in direct irradiation can be the major factor. The Fig3.8 shows a typical partly cloudy day.

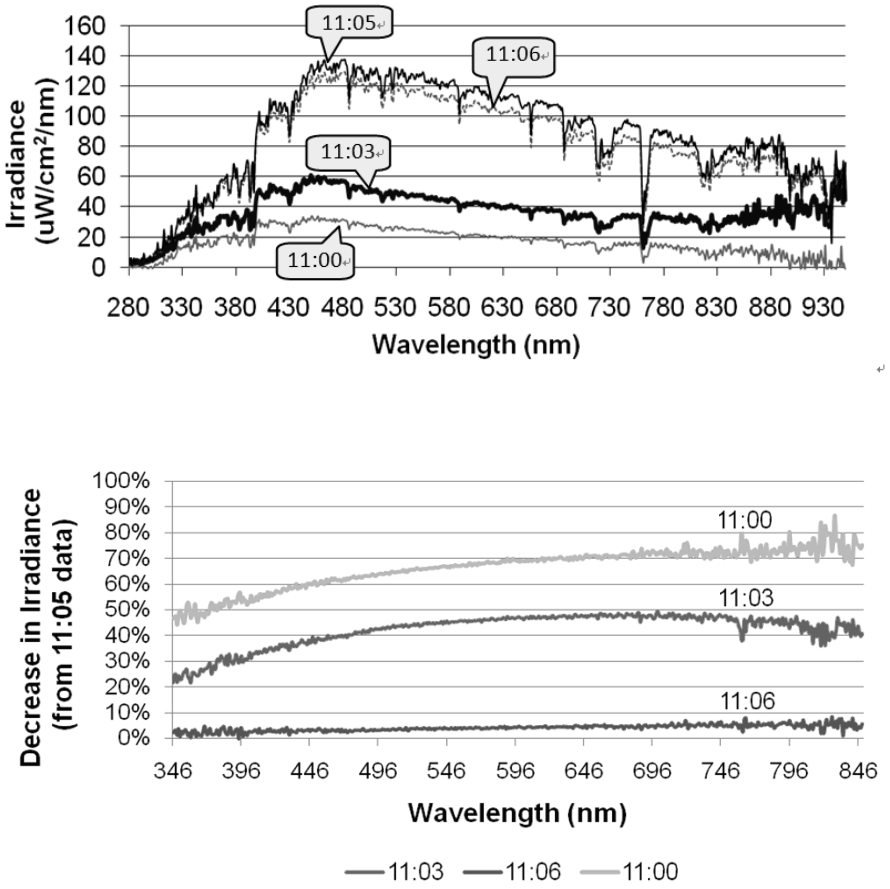

Fig3.8: The solar spectrum changed in a short period of time depending on the weather conditions. Clouds blocked the sun at 11:00 and 11:05, and it was partly cloudy from 11:03 to 11:06.

As shown in Figures 3.8, the solar spectra have the greatest variability in a short period of time and different weather conditions. These significant changes of solar spectra will play an important role in producing the electricity of solar cells.

In general, to identify and classify the different cloud coverage condition is to analyze the different types of solar irradiance spectra. This requests special equipment to recognize variable components of the solar irradiance

spectrum. Here is an example shown in Fig3.9. In other words, if the diffuse or direct radiance can be measured separately, then the variation of the diffuse and global irradiance will be plotted into one graph. Fig3.10 shows the variation of irradiance with time of day for four different sites under conditions of intermediate cloudiness. The bottom line is the diffuse component. The top line is the global component. When the two lines merge into one line, it is overcast, and the more difference the two lines have, the less cloudiness the sky is.

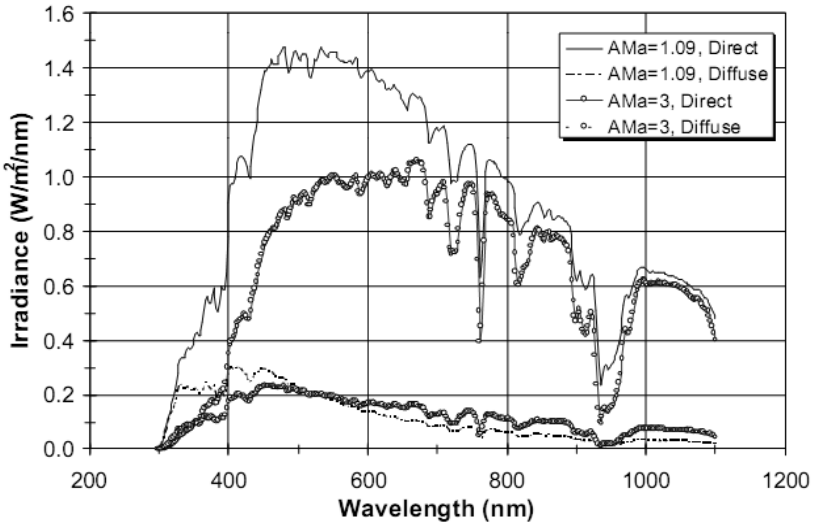

Fig3.9: Direct and diffuse solar spectral irradiance at the solar noon and at high AMa, Sacramento, CA [25].

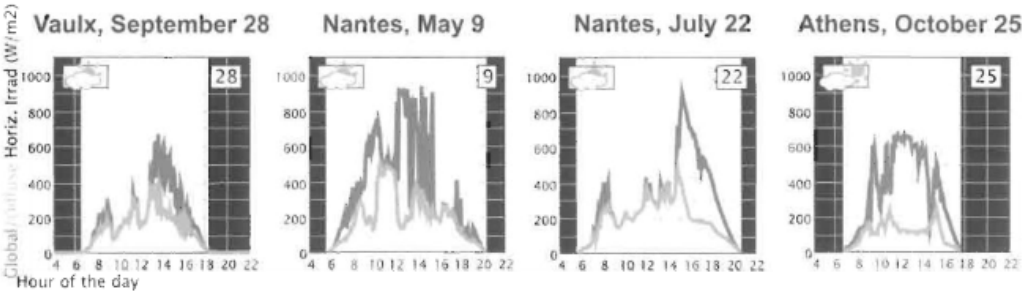

Fig 3.10: Variation of the global and diffuse irradiance with time of day for four different locations in Europe under conditions of cloudiness [26].

However, due to the limitation of the experimental equipments and the data handling ability, a more convenience way to compartmentalize different weather/sky conditions is to rely on the pyranometers. The advantage of the pyranometer is that the continuous solar insolation data can be achieve by programming with cRIO and Labview, and the sampling time intervals can be changed to fit the requirements. For instance, in the tropical climate as Hawai'i, the weather always change unpredictable and clouds are moving fast, we should measure as much as data to follow the quick changing, and take the average of a short period to present the weather/sky conditions.

Here is an example of one week in middle July.

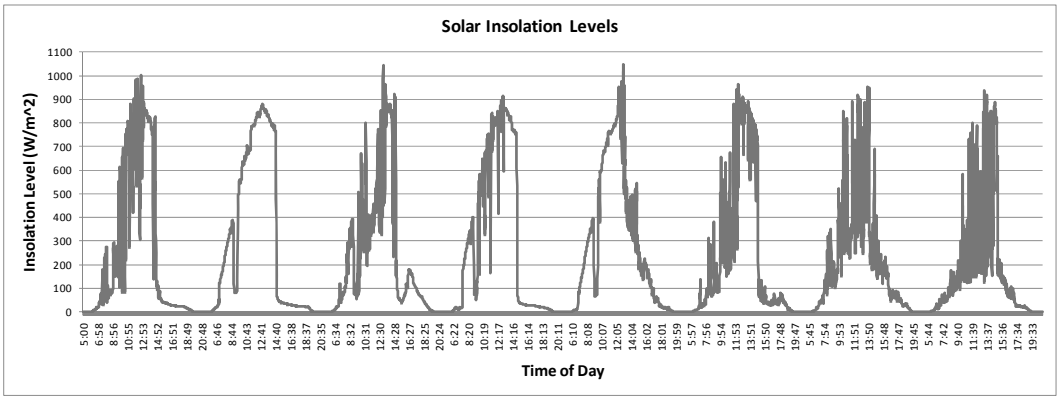

Fig 3.11: The Solar Insolation levels in middle July.

It can be seen in Fig3.11. The solar insolation levels measured from pyranometer on the roof of Holmes Hall were plotted in time order. The instantaneous weather variations can be observed intuitively from the plot. Notice that, the maximum insolation level always occurred at noon time which has the lowest Air mass value. The smooth curves illustrate the weather has less change during the day especially with Day Two; while the fluctuating curves mean the weather has a rapid change.

According to the observation of the skies and weather forecasts, empirical value of insolation level with different weather conditions can be summarized as the table below [27].

Table3.1: Insolation level with different weather conditions in the middle of July

	Insolation level (W/m2)		
Time of Day	Sunny	Partly Cloudy	Cloudy
9:00	600	400	100
13:00	1000	600	150
17:00	200	100	50

After the detailed measurements of the solar insolation are collected at the site of the installation, then we can combine those measurements with the weather forecast to predict the intensity just by observing the sky and to further estimate the output electricity of the solar cell. More details will be discussed in Chapter 5.

CHAPTER 4

Characterization of solar cells and Electrical Characteristics

4.1 Laboratory Solar Cell Performance Testing

4.1.1 Experimental setup

In the laboratory experimental research, the most crucial property to describe the performance of solar cells is electrical characteristics. The device J-V characteristics can be obtained under simulated solar illumination with both extraterrestrial and terrestrial simulated conditions using an ozone-free xenon bulb shined through either an AM0 or AM1.5G filter [28]. The light output power was calibrated by the spectroradiometer shown in Fig4.1 with the range from 250nm to 1100nm of wavelength and compared with the reference solar spectrum from the American Society for Testing and Materials (ASTM). To set a uniform measurement environment, the light output power will be first adjusted to the total insolation level by comparing the integrated measured irradiance of the light bulb to the integrated irradiance of the solar spectra. One example is presented in Fig4.2 for AM1.5G. Although there is a difference between the two curves, the integrated powers are both close to 81w/cm2. A silicon photodiode is also used to monitor the consistency of the irradiance from the solar simulator. For AM1.5G, the calibrated value of photodiode current is 2.03mA (measured at NREL under calibrated solar simulator). The output of the solar simulator can be easily regulated when fluctuations occurred to match the same current. To make the testing more approached the standard testing condition (STC), a cooling plate is placed to provide constant temperature (25° C). More details about the testing and operation standards of photovoltaic will be discussed in chapter 5.

a. b.

Fig4.1: Pictures of (a) The Xe ozone-free solar simulator and (b) PV cells electrical set up. In this picture, a 1"x1" sample is being tested. The reference Si-photodiode is located right next the sample to ensure that the irradiance is constant during the test.

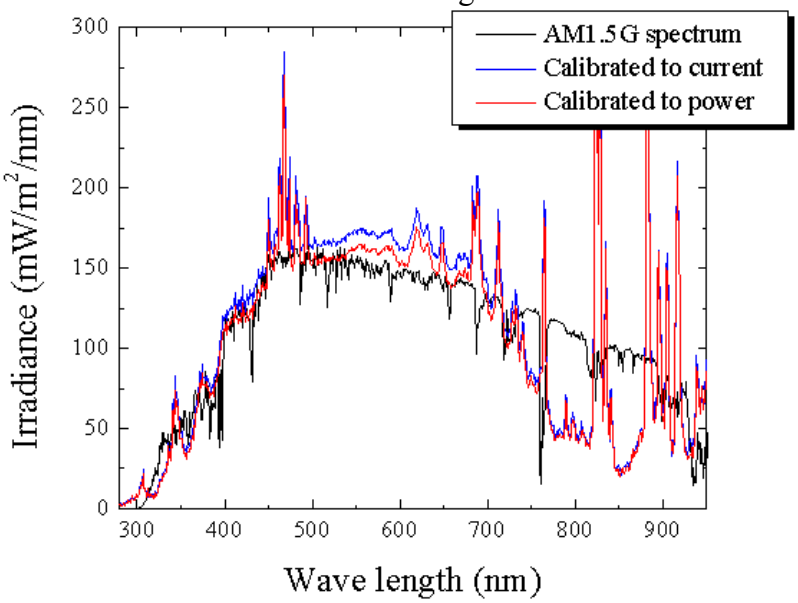

Fig4.2: The lab calibrated solar spectra from the solar simulation and the comparison with the AM1.5G reference spectrum.

4.1.2 Current-Voltage (J-V) Curve and other electrical parameters

Frequently, current versus voltage measurement means determination of the basic parameters open-circuit voltage, short-circuit current, Fill Factor and efficiency (ɳ), which are determined by only three points on the J-V curve. Since these parameters can be the indicators of solar cell performance, it is very important to analyze and compare the J-V curve with the dependence on solar intensity and temperature as a consideration in photovoltaic conversion modeling.

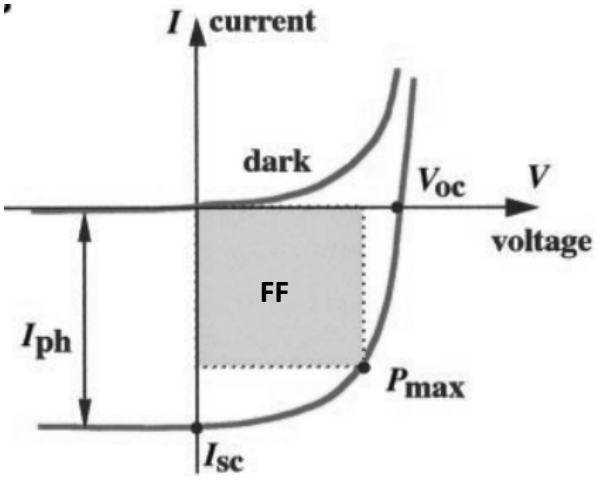

Fig 4.3: Typical J-V characteristics of a solar cell [29].

Where the three characteristic parameters: short- circuit current Jsc, open-circuit voltage Voc, and fill factor FF =Pmax /(Voc × Isc).

From the Fig4.3, the characteristics of the diode under nonilluminated condition are the dark curve. Compare with the photogenerated curve, in principle, be linearly superimposed [30]. The photogenerated current density Jph is the maximum limit for Jsc. The detail relational expression will be discussed in Chapter 5.

All these parameters can be achieved from the J-V measurement with the solar simulator. A typical CIGS J-V curve measured in the lab is shown in Fig 4.4 and with corresponding QE curves shown in Fig 4.5.

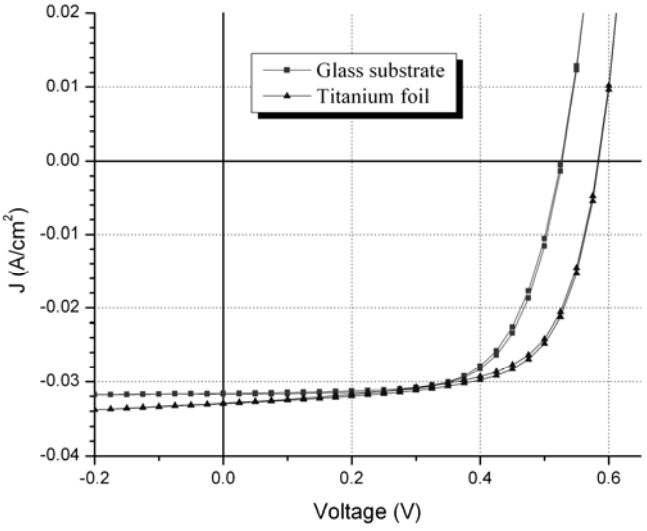

Fig 4.4: J-V curves of the CIGS cell with two different types of substrates.

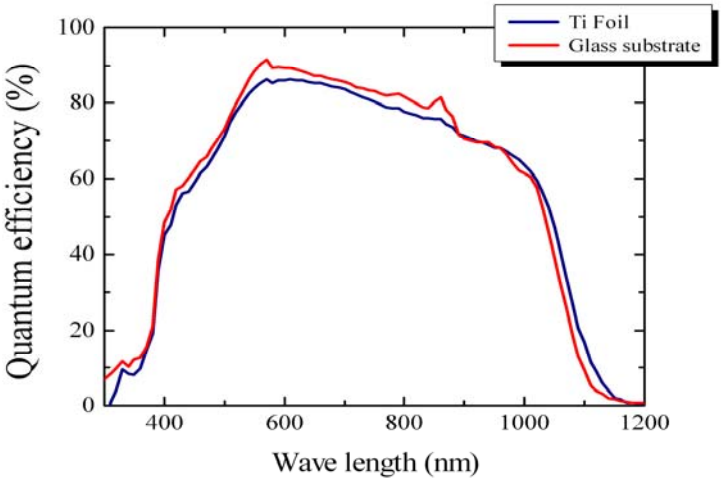

Fig4.5: JV and QE curves of the CIGS cell with two different types of substrates.

To simplify the result of J-V measurement, the J-V curves of three randomly selected samples will not be displayed, instead of their main electrical parameters list as in Table.

Table 4.1: The electrical parameters of three randomly selected samples.

Substrate ID	Efficiency %	FF	Voc	Jsc (mA/cm2)
CIGS_27 12 6	10.91	69.03	0.509	-3.12E-02
CIGS_27 31 3	10.44	56.96	0.596	-3.09E-02
CIGS_27 32 1	12.09	70.08	0.551	-3.14E-02

4.2 Estimate the Jsc from QE measurement

Short-circuit current density is a main characteristic to evaluate the performance of solar cell, and most of solar cell materials researchers have been applying themselves to increase the Jsc [31]. It can be validated from the Eq 4.1. Jsc is directly proportional to the efficiency η. Jsc can be measured from the J-V measurement with a solar simulator. However, if more precise results with real-time solar insolation would be expected, there is another way to derive the Jsc from QE measurement.

$$\eta = \frac{P_{out}}{P_{in} Ac} \cdot 100\% = \frac{I_{sc} V_{oc} FF}{P_{in} Ac} \cdot 100\% \qquad \text{Eq 4.1}$$

Recall that the definition of Quantum Efficiency, QE therefore relates to the response of a solar cell to the various wavelengths in the spectrum of light illumination. As it is known that the J-V measurement in the lab was processed under AM1.5G, to validate the same current density we could achieve from both methods, the AM1.5G spectrum will be used in the

calculation. Fig4.6 shows the QE of three CIGS samples mentioned above with J-V measurement.

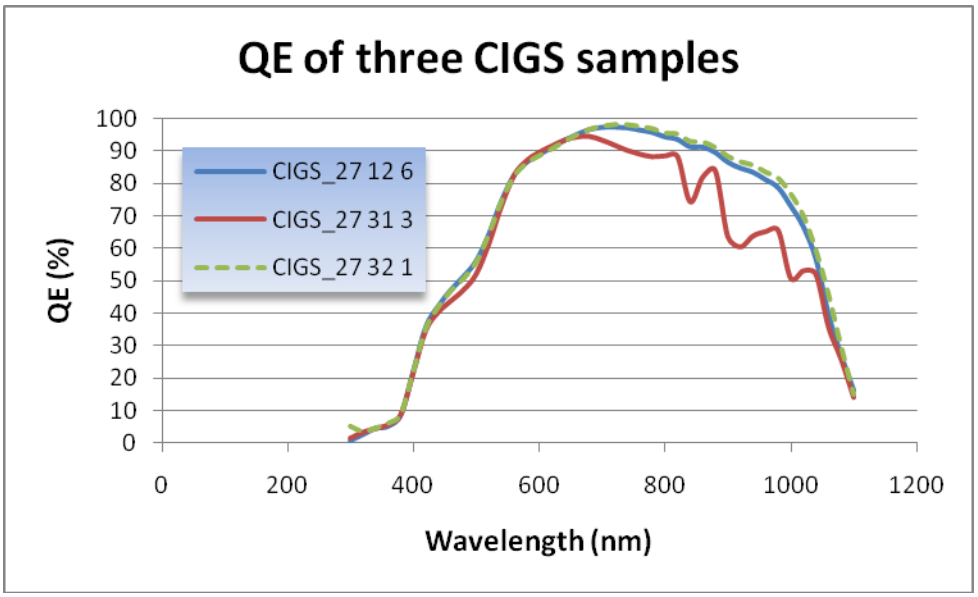

Fig4.6: Quantum Efficiency of three CIGS samples.

Table 4.2 shows the Jsc measured from J-V and calculated from QE. Notice that there is a deviation from two methods due to the non-uniformities from the solar simulator and QE measurement unit.

Table4.2: The current density of three samples from J-V and QE measurement

Substrate ID	Jsc from J-V (mA/cm2)	Jsc from QE (mA/cm2)
CIGS_27 12 6	31.2	32.76
CIGS_27 31 3	30.9	30.17
CIGS_27 32 1	31.4	33.07

As far as this estimate method is verified from J-V measurement, the AM1.5 spectrum can be substituted by the real-time solar spectrum. Although only the theoretical value is considered by the laboratory research, the real performance of solar cell under different weather condition will provide more accurate reference to the installation of photovoltaic panel.

An alternative approach to estimate the maximum short-circuit current density is to assume the material can absorb and convert 100% of light to electricity [32]. With Matlab program, integrate the AM1.5 spectrum by every wavelength, the maximum Jsc can be plotted as Fig4.7.

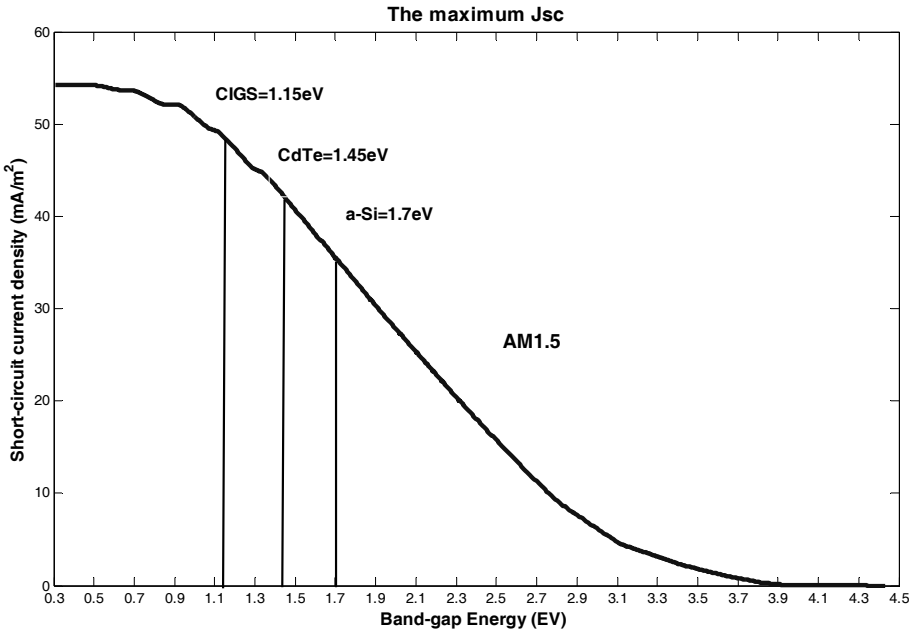

Fig 4.7: The maximum short-circuit current density with three different materials.

CHAPTER 5

Modeling of Photovoltaic Panel and Case Study

5.1 Temperature impact of solar cell

5.1.1 Performance rating method

We already discussed the effect of solar irradiance on the performance of the solar cell. To simulate the real condition of outdoor photovoltaic, the temperature factor needs to be considered as well.

The J-V curve of a photovoltaic device under illumination is a strong function of temperature, which must be accounted for in performance simulation. Typically, Jsc has the smallest temperature dependence, caused by the semiconductor band-gap shifting to longer wavelengths with higher temperature. Voc and Pmax, degrade rapidly with increasing temperature.

These strong dependencies are the reason a fixed temperature is used for Standard Reporting Conditions (SRC) [33]. There are two different reference spectral irradiances using as SRC, one with the total irradiance at 1366.1 W/m2 and at the temperature of 28° C; while the other with the total irradiance at 1000 W/m2 and at the temperature of 25° C (also referred to as standard testing conditions). It should be emphasized that the standardized spectral irradiances cannot be reproduced exactly in the laboratory. It becomes another reason which it is necessary to simulate the performance with real conditions of outdoors.

Although performance at SRC or STC is an important parameter to compare the performance between different PV devices, it is not a realistic indication of the performance that can be expected outdoors, where devices almost never operate at 25° C when the irradiance is greater than 900W/m2. Another method is called Performance Test Conditions (PTC), which with the

irradiance at 1000W/m2, at the ambient temperature of 20° C and with wind speed of 1 m/s. This method is usually used to simulate a system over a period of time if the conditions are close to the rating conditions.

In this experimental study, the simulation of photovoltaic used a translation of STC based on a number of parameters measured in the laboratory and outdoors. Temperature is an initial consideration in the modeling.

5.1.2 Temperature coordination

Ambient temperature

To integrate the measured temperature and corresponding spectral irradiance into the modeling, it is necessary to rate the module based on energy production rather than output power at a single fixed condition. An energy rating establishes five references days: hot-sunny, cold sunny, hot-cloudy, cold cloudy and nice. For the area like Hawai'i, the situation is simpler since it has a relatively constant temperature during the year. It can be obtained easily from the weather record.

As an individual input parameter, solar irradiance is easy to change for every single variation on different weather conditions and solar positions. However, the temperature impact is more complicate. The increasing of ambient temperature will decrease the efficiency of the solar cell.

Operating temperature of PV module

Above temperature is mainly described for ambient temperature, however, the cell temperature of the photovoltaic device is another factor. It is usually derived from ambient temperature. The Normal Operating Cell Temperature (NOCT) is defined as the cell temperature when irradiance is 800 W/m2,

ambient temperature is 20° C and wind speed is 1m/s. NOCT can be summarized by on site measurement of PV modules [35].

Here is the expression of cell temperature:

$$Tc = Ta + (NOCT - 20^{\circ}\ C) * \frac{G}{800} \qquad \text{Eq 5.1}$$

Where, Ta is ambient temperature, G is the solar insolation level. This equation provides a method to estimate the cell's operating temperature.

Temperature VS Isc and Voc

Assume operating temperature increase ΔT compare with the STC condition. Here the temperature coefficient will be applied in the calculation, temperature coefficient for Isc and Voc are usually assumed to be independent of the solar irradiance level. Although this assumption is not strictly correct, it is a reasonable simplification. There is less than 5% change in the voltage coefficients for a typical flat-plate module with solar irradiance varying from 100 W/m2 to 1000W/m2 [34]. The coordinated Isc and Voc are expressed as follow equations:

$$Isc(T)=Isc(Tr)*(1+\alpha * \Delta T) \qquad \text{Eq 5.2}$$

$$Voc(T)=Voc(Tr)*(1+\beta * \Delta T) \qquad \text{Eq 5.3}$$

Here Isc(Tr) is short-circuit current density at reference temperature, Voc(Tr) is the open-circuit voltage at reference temperature. α is the temperature coefficient for Isc and β is the temperature coefficient for Voc.

These temperature coefficients for small module can be measured with J-V in the laboratory by changing the temperature. For outdoor tests, it is also available by shading the module to reach the testing temperature. Both of the cases need to measure the average module temperature using adhere thermocouples attached to the rear surface.

For arrays of modules, it is usually impractical to measure the temperature coefficient directly. Alternatively, temperature coefficients for array can be estimated by the previously measured modules. These information can be easily obtain from the data base [35, 36].

5.2 Modeling Theory

5.2.1 PV module model

Mathematical Model of PV

Considering the reference of temperature T and solar radiation G. Fig 5.1 shows the simple equivalent circuit of a solar cell. It is a current source in parallel with one diode. The output of the current source is directly proportional to the photocurrent Iph. During the darkness, the solar cell is not active and it works as a diode. It produces no current. However, if it is connected to an external supply, the same purpose as the solar cell illuminated under the sun, and then it generates a current ID, called diode current. The I-V characteristic of the cell is determined by the diode. Fig 5.2 shows the relationship of these currents in electrical characteristic plot.

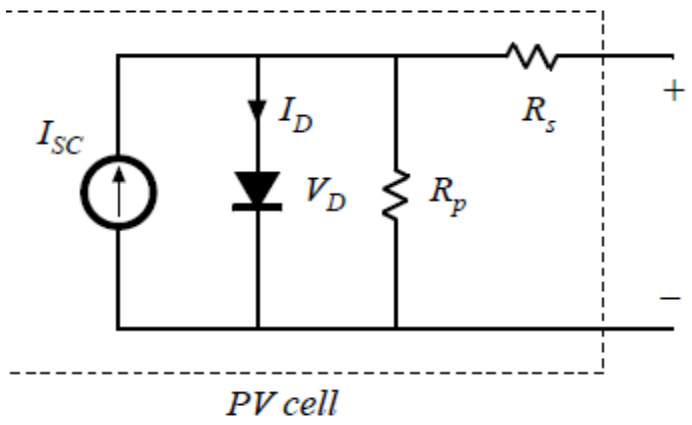

Fig5.1: The mathematical model of a single diode model [37]

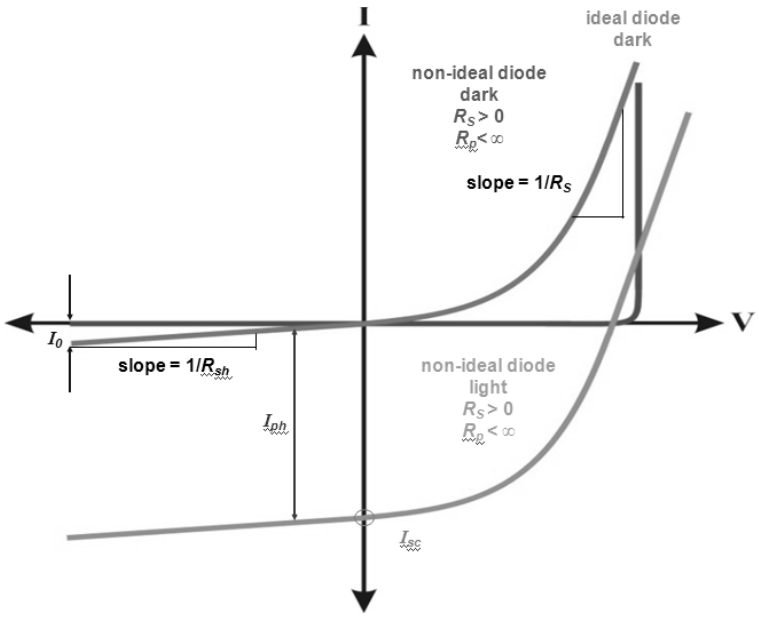

Fig 5.2: The electrical characteristic of solar cell.

Where,

The output current: $$I_{PV} = I_{SC} - I_D - \frac{V_D}{R_P}$$ Eq 5.3

The output voltage: $$V_{PVcell} = V_D - R_S I_{PV}$$ Eq 5.4

Diode characteristic: $$I_D = I_0 \left(e^{\frac{V_D}{V_T}} - 1\right)$$ Eq 5.5

Here Io is the temperature depended diode saturation current. V_T=KT/q is the thermal voltage.

Additional, the series resistance Rs in the model gives a more accurate shape between the maximum power point and the open-circuit voltage. This represents the internal losses due to the current flow. The shunt resistance Rsh, in parallel with the diode, corresponds to the leakage current to the ground and it is commonly neglected.

In the model of this study, an ideal cell Rs=Rsh=0 is used as a relatively common assumption.

5.2.2 Simulink of simple p-n junction photovoltaic module:

By using the Matlab Simulink program to simulate the simple p-n junction photovoltaic devices. The diode characteristic equation is in the model. The Fig shows the block diagram of the single diode model. The input variable is insolation level [38, 39].

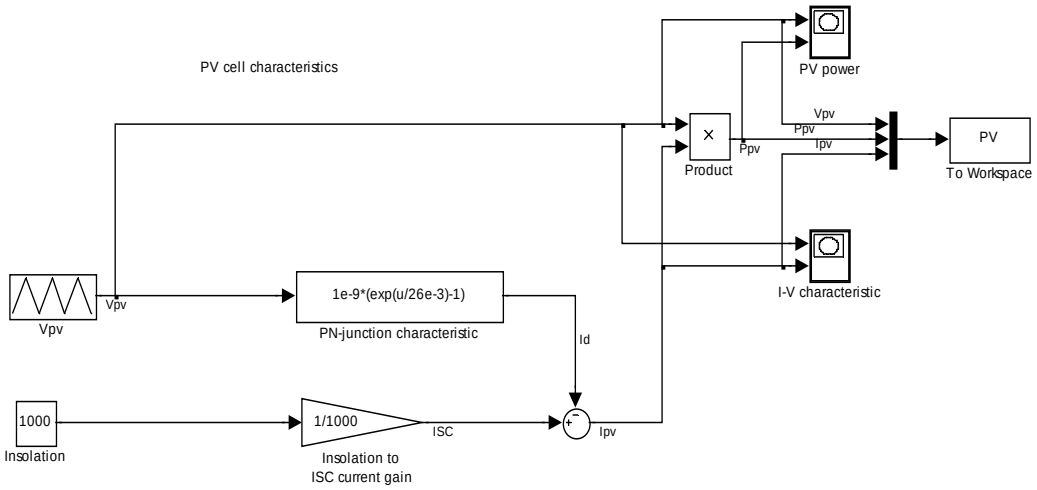

Fig 5.3: The Matlab Simulink block diagram of a single diode model of photovoltaic device.

The simulated result is shown as below. Because this simulation is under the condition of an ideal diode, the quantitative analysis will not be discussed instead of the qualitative analysis will be expressed.

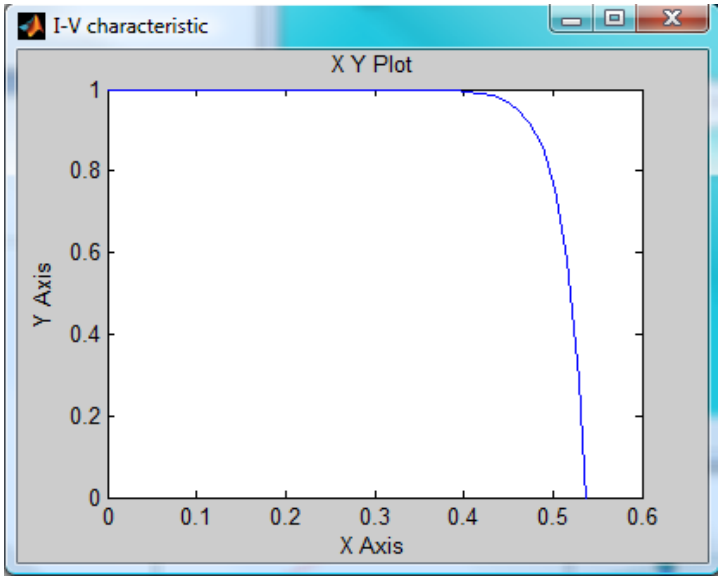

Fig 5.4: The screenshot of I-V curve from the simulation.

It is very important to analyze the trend of the I-V curve. Fig 5.5 is a normalized I-V plot. It should be pointed out that the power delivered to the load depends on the value of the resistance only.

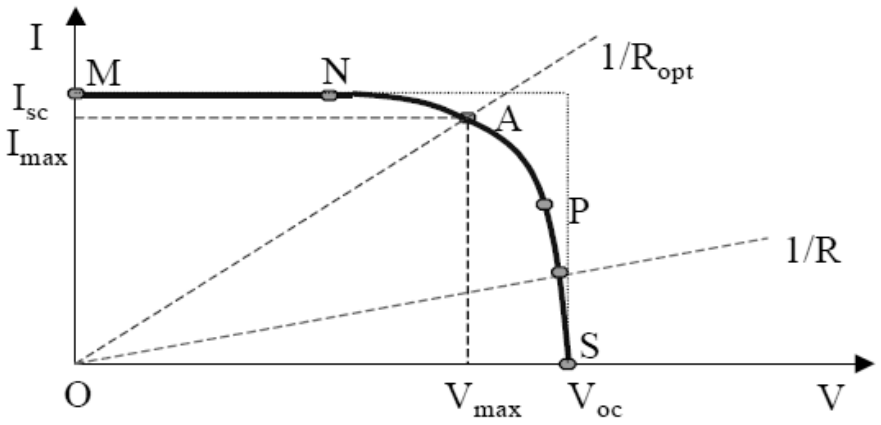

Fig 5.5: The I-V characteristic of the solar cell for a certain ambient irradiation G and a certain fixed cell temperature T [38].

The cell's terminals are connected to a variable resistance R, the operating point is determined by the intersection of the I-V characteristic. For a resistive load, the load characteristic is a straight line with a slope 1/R.

M-N Curve:

If the load R is small, the cell operates in the region MN of the curve, where the cell behaves as a constant current source, almost equal to the short circuit current. It is the greatest value of the current generated by a cell, which the conditions: V=0.

P-S Curve:

If the load R is large, the cell operates in the region PS of the curve, where the cell behaves as a constant voltage source, almost equal to the open- circuit current.

Open circuit voltage corresponds the voltage drop across the diode, when the generated current is I=0. It reflects the voltage of the cell in the night.

Here $$V_{OC} = V_T \ln\left(\frac{I_{PV}}{I_O}\right)$$ Eq 5.6

N-P Curve:

Maximum power point is the operation point A, at which the power is the maximum: $$P_{max} = I_{max} * V_{max}$$ Eq 5.7

The maximum efficiency is the ration between the maximum power and the incident light power also occurred at point A. Fill factor is the ratio of the maximum power that can be delivered to the load and the product of Isc and Voc. Usually, this value can reach to 0.7 for a good cell.

5.3 Case Study

5.3.1PV panel installation and specific parameters of modules

In this study, the Green Holmes Hall Initiative (GHHI) project was involved. UH Holmes Hall is an engineering building which has large amount electricity consumption laboratory and computer lab in it. A statistic report from Facilities Management Office revealed that the energy usage of Holmes Hall was 5,558,000 kWh/yr as of 2008 which work out to about 634kW of energy consumption on average. The installation of photovoltaic panels would help to reduce the cost of electricity bill. Fig 5.6 is a satellite top view map of Holmes Hall roof area. So far, the PV panels of GHHI have already settled on the south-east of the roof (pointed on Fig 5.6). Fig 5.7 shows the two different types of PV panels. Every 100 square feet of roof area would produce approximate 1kW of energy [40]. Holmes Hall has about 30,000 square feet of usable roof area. In that case, we could only produce 300kW from solar energy during the day. This potion is only 50% of total energy consumption. The general limitation of the available roof area becomes a driving force using higher efficiency photovoltaic technologies.

Fig 5.6: The satellite top view map of Holmes Hall roof area with the pointed PV installation area.

Fig 5.7: The actual PV panels installed on UH Holmes Hall roof. The Model # MHI_MT_130 (a-Si) from Mitsubishi is on the left while the right one is from Kyocera, Model # KD205GX-LP (p-Si).

Since a single PV cell produces an output voltage of less than 1 volt, it is necessary to string together a number of PV cells in series to achieve a desired output voltage. The Mitsubishi MHI_MT_130 PV panels contain 6 parallels of 4 series connected single modules which can provide 570V-2A energy output per branch. The total electricity generation would reach to 3kW. The

Kyocera KD205GX-LP PV panels contain 2 parallels of 13 series connected single modules which can provide 470V-9A per branch. The total electricity generation would reach to 5kW. This total 8kW DC system is project to produce 45-55kWh per day on average based on an average 5-7 kWh production for every 1kwdc of PV.

The data sheets for both types provide the following information on the module:

Table5.1. The spec sheet of Mitsubishi MHI 130 module [42].

Electrical characteristics	Stabilised value	Initial value (maximal)
Nominal power (P_{nom})	130 Wp	+8%
Power tolerance	± 5%	
Voltage at max. power point (U_{mpp})	101 V	+3%
Current at max. power point (I_{mpp})	1,29 A	+5%
Open-circuit voltage (U_{oc})	131 V	+1%
Short-circuit current (I_{sc})	1,53 A	+2%
Maximum system voltage	600 V	
Operating module temperature	- 20°C to + 85°C	

The electrical data apply to standard test conditions (STC): Irradiance 1000 W/m², module temperature 25°C, AM=1.5
The rated power may vary by ± 5% and all other electrical parameters by ± 10%.

Temperature coefficients	
Power T_K (P_n)	- 0,28%/°C
Open-circuit voltage T_K (U_{oc})	- 0,32%/°C
Short-circuit current T_K (I_{sc})	+ 0,06%/°C

Table5.2. The spec sheet of Kyocera KD205GX-LP module [43]

■ Electrical Performance under Standard Test Conditions (*STC)	
Maximum Power (Pmax)	205W (+5%／−5%)
Maximum Power Voltage (Vmpp)	26.6V
Maximum Power Current (Impp)	7.71A
Open Circuit Voltage (Voc)	33.2V
Short Circuit Current (Isc)	8.36A
Max System Voltage	600V
Temperature Coefficient of Voc	−0.120 V/℃
Temperature Coefficient of Isc	5.02×10^{-3} A/℃

*STC : Irradiance 1000W/m^2, AM1.5 spectrum, cell temperature 25℃

■ Electrical Performance at 800W/m^2,*NOCT, AM1.5	
Maximum Power (Pmax)	145W
Maximum Power Voltage (Vmpp)	23.5V
Maximum Power Current (Impp)	6.17A
Open Circuit Voltage (Voc)	29.9V
Short Circuit Current (Isc)	6.82A

*NOCT (Nominal Operating Cell Temperature) : 49℃

Their electrical characteristics are shown in Fig5.8 and Fig 5.9.

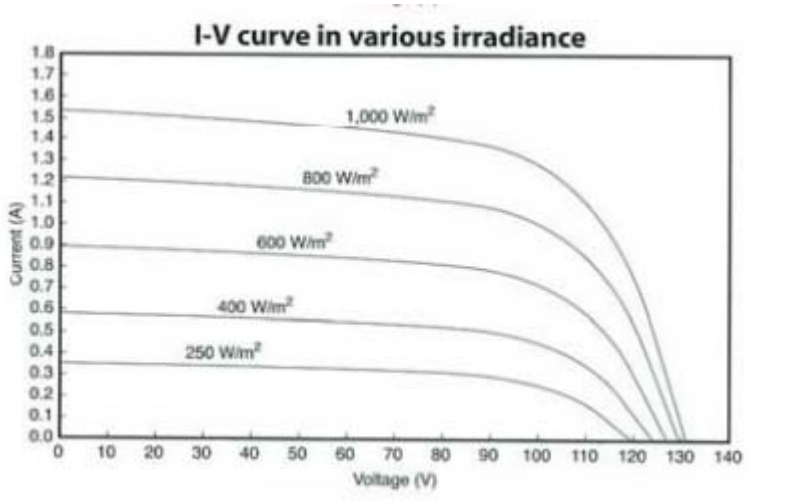

Fig 5.8. The I-V curve of Mitsubishi module under STC.

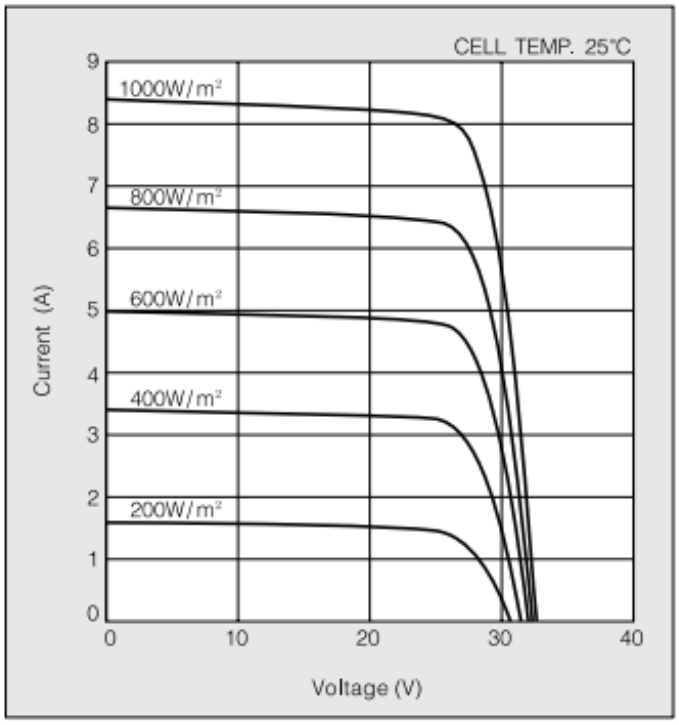

Fig 5.9. The I-V curve of Kyocera module under STC

5.3.2 Simulation and Validation

Currently, only the modules from Mitsubishi are connected with the grid providing electricity to the building. An important goal of the GHHI project isthe evaluation of the performance of differentphotovoltaic modules. Here, the simulation model has been designed based on single diode model and applied to validate the specifications of photovoltaic devices which provided by the manufacturers.

In order to simulate the system(s) under real-time conditions, it is convenient to make the assumptions of several typical circumstances to represent different weather conditions in December as in Hawai'i. It is informative to take the Mitsubishi module as an example, evaluated under the three simulation cases listed below.

1. Sunny day: Insolation level at 1000 W/m2 and temperature at 26° C.
2. Partly cloudy day: Insolation level at 550 W/m2 and temperature at 24° C.
3. Cloudy day: Insolation level at 120 W/m2 and temperature at 22° C.

After the calculation, the table5.3 shows the cell temperature and correlated Isc and Voc for both PV panels.

Table 5.3 : The calculated result of cell temperature and Isc and Voc.

	Mitsubishi MHI_MT_130		
	Case 1	**Case 2**	**Case 3**
Tc (° C)	35.89	34.62	22.68
Isc (A)	1.57	1.55	1.54
Voc (V)	113.1	119.7	124.3

Then using the Matlab simulink program, the output plots for one single module with three weather conditions are shown below in Fig5.10.

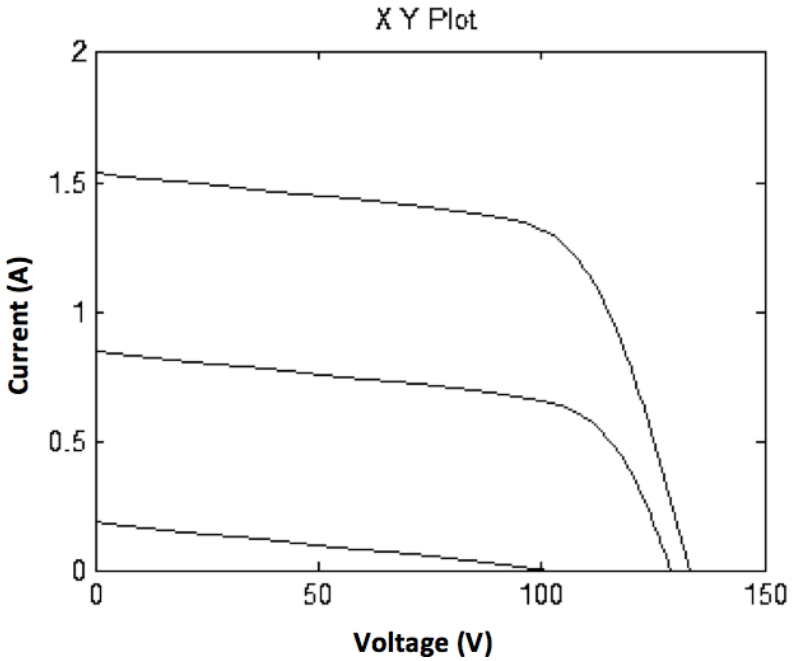

Fig5.10. I-V curves under three different weather conditions with different insolation levels (ascending order as 120W/m2, 550W/m2 and 1000W/m2)

The simulation results approach to the standard data as insolation approaches 1000W/m2. Compared with the STC situation, the impact of temperature can be significant smaller than the solar irradiance since the temperature fluctuation is small in Hawai'i. The estimated power output is listed in Table 5.4.

Table 5.4. Insolation and power output of the module.

	Sunny	Partly Cloudy	Cloudy
Insolation (W/m2)	1000	550	120
Power output (W)	3012.53	1593.91	311.74

It is necessary to point out that the power is in direct proportion to the insolation level.

5.3.3 Accurate Quantum Efficiency Estimation

In order to avoid the errors from spectral mismatch of solar simulators which measured the short-circuit current density and to present a more accurate value with real-time spectral irradiance, A mathematical model was designed to calculate Jsc by multiplication of the measured quantum efficiency curves with the measured actual solar spectrum, and subsequent integration from 300-1150nm.

This estimation, also processed within three different weather conditions as mentioned above. Fig5.11, shows the spectral sensitivities of solar cells to these three conditions.

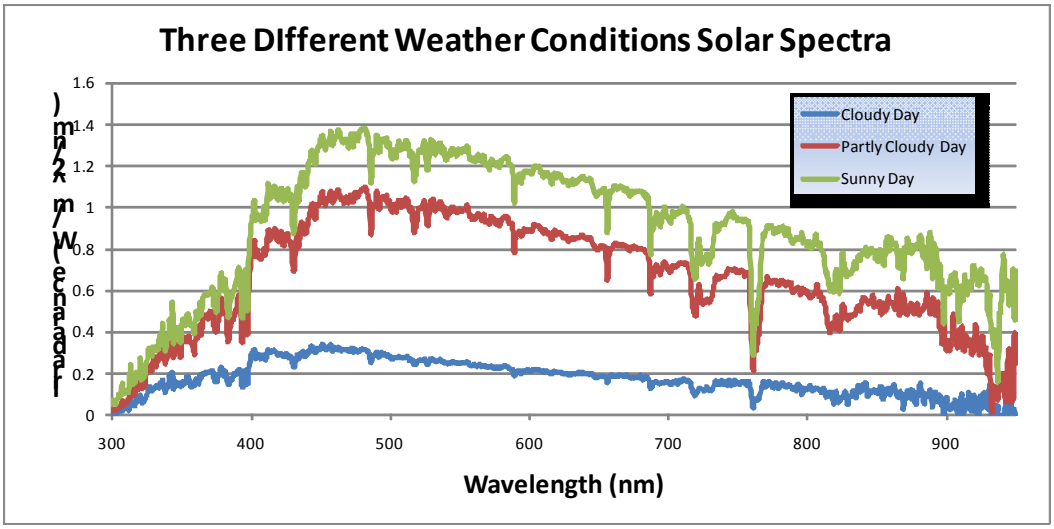

Fig 5.11. Three solar spectra of different weather conditions.

The Mitsubishi MHI module used micromorph tandem solar cells. Micromorph silicon is a combination of amorphous silicon (a-Si) and microcrystalline silicon (μ c-Si) which absorb the sunlight of the solar spectrum for wavelength in the range from ultraviolet to infrared light (250nm to1100nm). Because of its tandem structure, the light will be absorbed by the first layer (a-Si) and the rest of the light will continue illuminate the second layer (μ c-Si), the currents generated by both layer should be match-up. The quantum efficiency curve from literature is shown in Fig5.12.

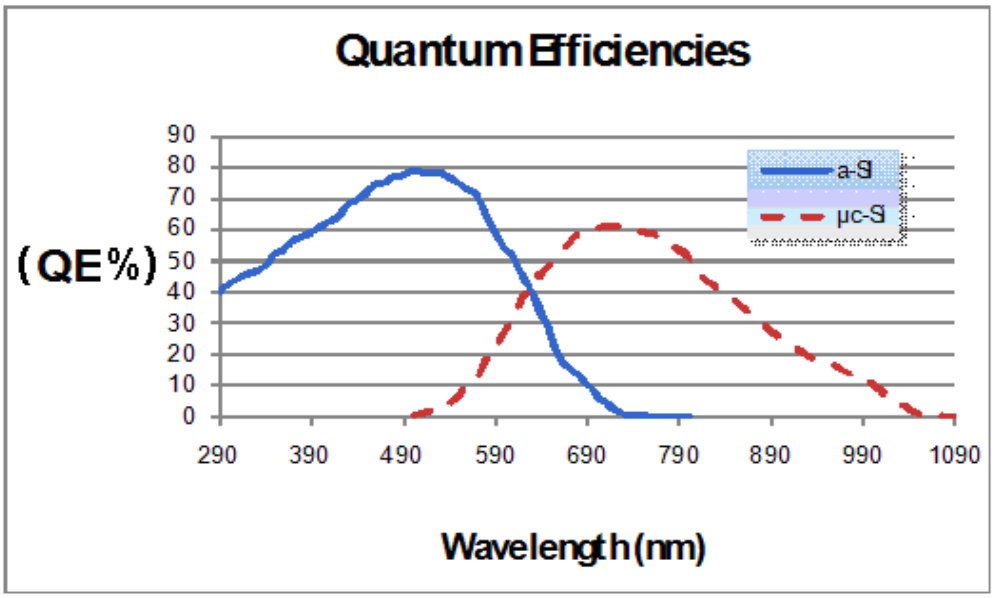

Fig 5.12 The Quantum Efficiency of micromorph silicon material [44].

Compare with crystalline silicon, the micromorph module will produce more electricity at cloudy conditions and dawn, and the light induced initial degradation of micromorph modules is significantly weaker than amorphous silicon [42].

The Kyocera module used polycrystalline silicon material (p-Si). Polycrystalline silicon is the dominated material in the photovoltaic market so far. Compare to other thin film amorphous silicon photovoltaic technologies, polycrystalline silicon does not suffer from light-induced degradation, and compared to crystalline silicon technologies, it has lower cost. [45]. A typical p-Si quantum efficiency curve is shown in Fig5.13.

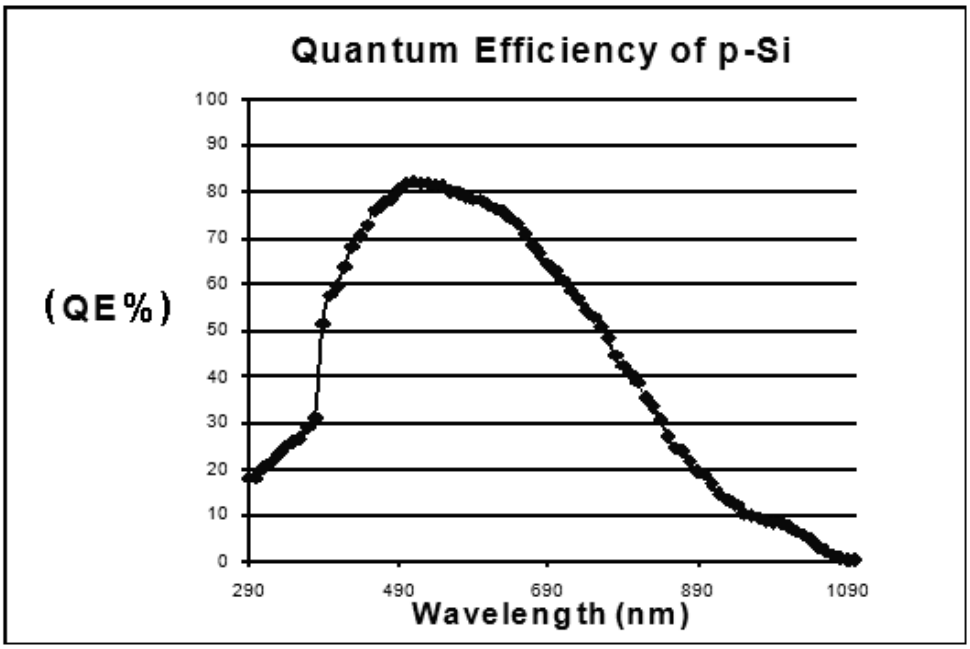

Fig5.13 The Quantum Efficiency of polycrystalline silicon material [45].

The third device modeled is based on CIGS material, as detailed in previous sections. CIGS solar cells have been researched and developed for almost a decade. Nowadays, more and more thin-film labs and photovoltaic manufactories are focusing on the development of CIGS solar cell. The highest efficiency achieved is approximately 19.9% achieved on a laboratory scale [46].

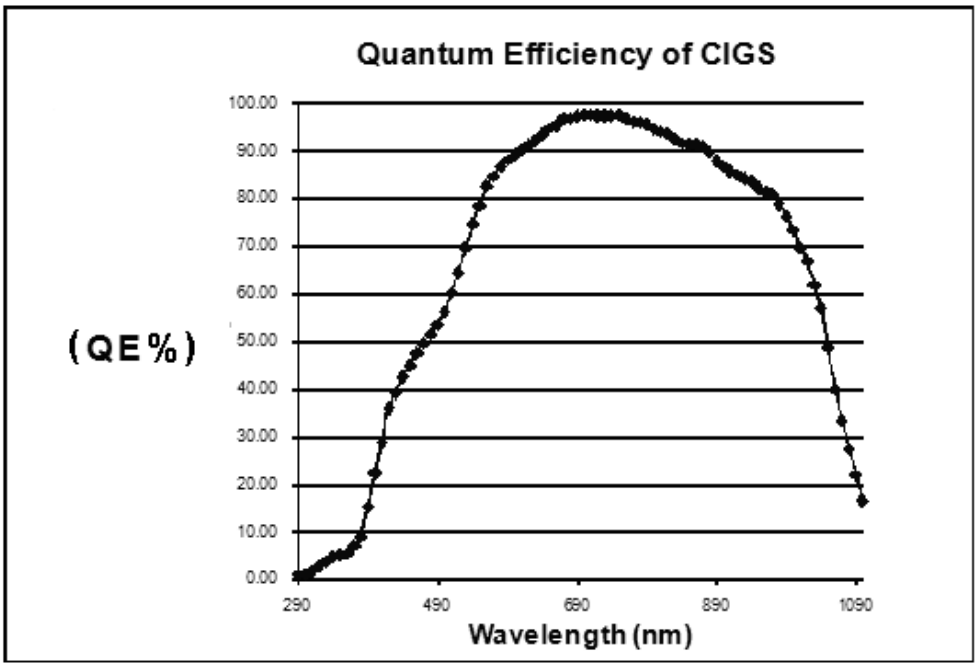

Fig 5.14 The Quantum Efficiency of CIGS material.

After the calculation, the result of short-circuit current density Jsc is listed in Table 5.5.

Table 5.5 The short-circuit current of three photovoltaic materials with three different weather conditions and an AM1.5 spectrum condition (Unit: mA/cm^2).

	Sunny day	Partly Cloudy	Cloudy Day	AM1.5
Micromorph	9.39	7.31	2.06	11.27
P-Si	16.70	12.45	3.16	20.58
CIGS	26.13	17.94	4.10	32.64

From the Eq. 4.1, it is clear that the Jsc is in direct proportion to the efficiency. This is a better alternative method to estimate the efficiency within

the consideration of measured spectral irradiance and measured quantum efficiency. Compare with the reference condition (AM1.5), am empirical conversion ratio can be derived and it will be used as further calculation of power output and energy conversion efficiency.

From the table, it can be seen that, the micromorph and polycrystalline silicon have a similar performance. CIGS has a significant higher Jsc, but it is also less commercially developed than the other two materials.

In the near future, the photovoltaic industry needs to identify the trade-off points between the expense and energy conversion efficiency depending on the available installation area and specific climate characteristic. In that case, it is necessary for the photovoltaic device manufactories to provide a more exhaustive specification report.

5.4 Modeling Summary

Using the real-time scale to simulate the photovoltaic system would be a good method to estimate the efficiency of modules and validate the performance specifications provided by the manufactories. A more accurate method considering the spectral response of the materials to derive the short-circuit current of the solar cell is also be expressed. These simulation results will become a crucial determinant in PV panel installation especially with the very limited roof area.

Chapter 6

Summary and Conclusions

The purpose of this experimental study is to provide a reference to photovoltaic users for the selection of photovoltaic modules by simulative and mathematical methods. Depending on the different climate conditions, available photovoltaic installation area and energy demand, the users can find a trade-off point between materials characteristic, covering area and cost. In this experimental study, a solar data acquisition system was designed and completed with two different types of solar sensors. The spectral irradiance and insolation levels are measured to assist the further experiment and modeling. A series of measurement has been done in the lab since it is necessary to achieve the optical and electrical properties of solar cells. Quantum Efficiency (QE) is an important optical characteristic which is relevant to the solar spectra. It is a good attempt to derive the short-circuit current density (Jsc) from the measured QE with the consideration of spectral irradiance. A mathematical model in this study was built to estimate the ratio of energy conversion since the Jsc is in direct proportion to the efficiency. In addition, a simulative model was also designed regarding to Green Holmes Hall Initiative project. This model can simulate the electricity output situation with real-time illumination and temperature. Combine these two works together offers some new direction in evaluating the appropriateness of different photovoltaic technologies under different meteorological conditions. Both the developer and user will find a balance to accommodate the energy demand and consumption.

Also, if a long-term solar resource measurement can be sustained, the solar spectra could become a reference document used in multiple aspects such as weather prediction and solar energy.

References

1. Zekai Sen. Solar Energy Fuadamentals and Modeling Techniques. Springer, 2008. P47.
2. Zekai Sen. Solar Energy Fuadamentals and Modeling Techniques. Springer, 2008. P55.
3. Zekai Sen. Solar Energy Fuadamentals and Modeling Techniques. Springer, 2008. P66.
4. Stefan Krauter. Solar Electric Power Generation. Springer, 2006. P121.
5. Zekai Sen. Solar Energy Fuadamentals and Modeling Techniques. Springer, 2008. P63.
6. Gilbert M. Masters. Renewable and Efficient Electric Power System. Wiley, 2004. P450.
7. Hans J. Moller. Semiconductors for solar cell. 1993. P11
8. Antonio Luque and Steven Hegedus. Handbook of photovoltaic science and engineering. 2002. P71.
9. Edward D. Palik. Handbook of Optical Constants of Solids. Academic Press NY. 1985.
10. Janes Krc, Franc Smole, and Marko Topic , Improving thin-film solar cells through optical modeling
11. Markus E. Beck. Solar Cell Fundamentals & CIGS-based Photovoltaic Devices. 2001
12. Gilbert M. Masters. Renewable and Efficient Electric Power System. Wiley, 2004. P459.
13. Steven S.Hegedus* and William N. Shafarman , Thin-Film Solar Cells: Device Measurements and Analysis

14. Johanna Schmidtke* Lux Research Inc., Commercial status of thin-film photovoltaic devices and materials , 234 Congress Street, Fifth and Sixth Floors, Boston, MA 02110, USA
15. M.I.Alonso et al. Optical functions of chalcopyrite CuGaxIn1-xSe2alloys.
16. T.J.Pease,D.P.Oxley,F.J.Clough. Low Temperature(≤150℃)a-Si:H films for large area electronic applications.
17. S. Saha et al. Optical Properties of CdTe Thin films.
18. S. Sirohi et al. Bandgaps of cadmium telluride sintered film.
19. CdTe-based Thin Film Solar Cell Research at the Institute of Energy Conversion.
20. Vipin Kumar a, Sachin Kr. Sharma a, T.P. Sharma a.*, V,Singh b , Band gap determination in thick films from reflectance measurements
21. J.J.Perez-Lopez*,F.Fabero and F.Chenlo , Experimental Solar Spectral Irradiance Until 2500nm:Results and Influence on the PV Conversion of Different Materials
22. David L. King, William E. Boyson, Barry R. Hansen, and Ward I. Bower Sandia National Laboratores , IMPROVED ACCURACY FOR LOW-COST SOLAR IRRADIANCE SENSORS
23. Kuo-Nan Liou , On the Absorption, Reflection and Transmission of Solar Radiation in Cloudy Atmospheres.
24. STEFAN NANN and CAROL RIORDAN , Solar Spectral Irradiance under Clear and Cloudy Skies: Measurements and a Semiempirical Model(Manuscript received 19 June 1990, in final form 8 October 1990)
25. David L. King, Jay A. Kratochvil, and William E. Boyson. Measuring Solar Spectral and Angle-of-Incidence Effects on Photovoltaic Modules and Solar Irradiance Sensor.

26. Tom Markvart. Practical Handbook of Photovoltaics Fundamentals and Applications.Elsevier. 2003. P79.
27. Chakradhar Lingamgunta, T. Nejat Veziroglu *, A universal relationship for estimating daily clear sky insolation.
28. The phase report of Thin Film Lab, HNEI, UHM. 2010.
29. A. Shah et al. Photovoltaic Technology: The Case for Thin-Film Solar Cells.
30. R. Gottschalg a.*, T.R. Betts a, D.G. Infield a, M.J. Kearney b , The effect of spectral variations on the performance parameters of single and double junction amorphous silicon solar cells.
31. M. Chandramohan a.*, S. Velumani b, T. Venkatachalam c.1 , Experimental and theoretical investigations of structural and optical properties of CIGS thin films.
32. T. Brammer*, W. Reetz, N. Senoussaoui, O. Vetterl, O. Kluth, B. Rech, H.Stiebig, H. Wagner , Optical properties of silicon-based thin-film solar cells in substrate and superstrate configuration.
33. David L. King, Jay A. Kratochvil, and William E. Temperature coefficients for PV modules and arrays: measurement methods, difficulties, and results.
34. M.Mattei,G.Notton*,C.Cristofari,M.Muselli,P.Poggi , Calculation of the polycrystalline PV module temperature using a simple method of energy balance.
35. M. Mattei, G. Notton*, C. Cristofari, M. Muselli, P.Poggi , Calculation of the polycrystalline PV module temperature using a simple method of energy balance
36. Ruhi Bharti et al. Normal Operating Cell Temperature (NOCT): Effects of module size, power, load and solar spectrum.

37. Ruhi Bharti et al. Nominal Operating Cell Temperture(NOCT):Effects of module size ,power ,load and solar spectrum.
38. Dzung D Nguyen and Brad Lehman, Modeling and Simulation of Solar PV Arrays under Changing Illumination Conditions, Department of ECE, Northeastern University.
39. Francisco M.Gonzalez-Longatt , Model of Photovoltaic Module in Matlab.
40. B. Marion, A Method for Modeling the Current-Voltage Curve of a PV Module for Outdoor Conditions.
41. University of Hawaii at Mānoa Energy Strategy 2008-2015
42. Mitsubishi MHI_MT 130 photovoltaic module specification sheet.
43. Kyocera KD205GX-LP photovoltaic module specification sheet.
44. Ralf Wehrspohn et al. Tandem solar cells with integrated intermediate reflectors.
45. Q. Kunz et al. 5% Efficient Evaporated Solid-phase Crystallised Polycrystalline Silicon Thin-film Solar Cells.
46. I, Repins et al. Characterization of 19.9%- Efficiency CIGS Absorbers.

Appendix

Matlab code of Tauc Plot

```
%load data from excel
final=xlsread('Tauc.xls');
T=final(:,8);
R=final(:,9);
E=final(:,3);
%input T=Io/I2,R,thickness nm
t=input('thickness=')
Alpha=abs((-1./t).*log(T./((1-R).^2)))
save Alpha
Alphai=min(Alpha)
subplot(131), plot(E,Alpha);
xlabel('hv'), ylabel('a')
grid on
%get direct bandgap
subplot(132), plot(E,(Alpha.*E-Alphai.*E).^2,'black');
xlabel('hv'), ylabel('((a-ai)hv)^2')
grid on
title('direct')
%get indirect bandgap
subplot(133), plot(E,((Alpha-Alphai).*E).^0.5,'red')
xlabel('hv'), ylabel('((a-ai)hv)^2')
grid on
title('indirect')
```